

# Lawrence Berkeley National Laboratory

## Recent Work

### **Title**

Nonlinear optical studies of liquid crystals and polymers

### **Permalink**

<https://escholarship.org/uc/item/59419954>

### **Author**

Hong, Seok-Cheol

### **Publication Date**

2002-06-30



# ERNEST ORLANDO LAWRENCE BERKELEY NATIONAL LABORATORY

## Nonlinear Optical Studies of Liquid Crystals and Polymers

Seok-Cheol Hong

Materials Sciences Division

June 2002

Ph.D. Thesis



Lawrence Berkeley National Laboratory  
Library Annex Reference

REFERENCE COPY |  
Does Not |  
Circulate |  
Copy 1

#### **DISCLAIMER**

This document was prepared as an account of work sponsored by the United States Government. While this document is believed to contain correct information, neither the United States Government nor any agency thereof, nor The Regents of the University of California, nor any of their employees, makes any warranty, express or implied, or assumes any legal responsibility for the accuracy, completeness, or usefulness of any information, apparatus, product, or process disclosed, or represents that its use would not infringe privately owned rights. Reference herein to any specific commercial product, process, or service by its trade name, trademark, manufacturer, or otherwise, does not necessarily constitute or imply its endorsement, recommendation, or favoring by the United States Government or any agency thereof, or The Regents of the University of California. The views and opinions of authors expressed herein do not necessarily state or reflect those of the United States Government or any agency thereof, or The Regents of the University of California.

This report has been reproduced directly from the best available copy.

Ernest Orlando Lawrence Berkeley National Laboratory  
is an equal opportunity employer.

## **DISCLAIMER**

This document was prepared as an account of work sponsored by the United States Government. While this document is believed to contain correct information, neither the United States Government nor any agency thereof, nor the Regents of the University of California, nor any of their employees, makes any warranty, express or implied, or assumes any legal responsibility for the accuracy, completeness, or usefulness of any information, apparatus, product, or process disclosed, or represents that its use would not infringe privately owned rights. Reference herein to any specific commercial product, process, or service by its trade name, trademark, manufacturer, or otherwise, does not necessarily constitute or imply its endorsement, recommendation, or favoring by the United States Government or any agency thereof, or the Regents of the University of California. The views and opinions of authors expressed herein do not necessarily state or reflect those of the United States Government or any agency thereof or the Regents of the University of California.

# **Nonlinear Optical Studies of Liquid Crystals and Polymers**

Seok-Cheol Hong  
Ph.D. Thesis

Department of Physics  
University of California, Berkeley

and

Materials Sciences Division  
Ernest Orlando Lawrence Berkeley National Laboratory  
University of California  
Berkeley, CA 94720

June 2002



# **Nonlinear Optical Studies of Liquid Crystals and Polymers**

Copyright © 2002

by

Seok-Cheol Hong

The U.S. Department of Energy has the right to use this document  
for any purpose whatsoever including the right to reproduce  
all or any part thereof.

**Nonlinear Optical Studies of Liquid Crystals and Polymers**

by

Seok-Cheol Hong

B.S. (Seoul National University, Seoul) 1995

A dissertation submitted in partial satisfaction of the  
requirements for the degree of  
Doctor of Philosophy

in

Physics

in the

GRADUATE DIVISION

of the

UNIVERSITY of CALIFORNIA at BERKELEY

Committee in charge:

Professor Y. R. Shen, Chair

Professor P. Y. Yu

Professor G. A. Somorjai

Fall 2002

## Abstract

Nonlinear Optical Studies of Liquid Crystals and Polymers

by

Seok-Cheol Hong

Doctor of Philosophy in Physics

University of California at Berkeley

Professor Y. R. Shen, Chair

Polymers are indispensable in our life. A life is a continuous event maintained by many complex processes in which biological polymers participate. It also gets help from a variety of natural and synthetic polymers with useful functions. Such functions depend on the chemical and conformational structures of polymers and often largely on the surface structures and properties of polymers

We used second order nonlinear optical techniques (sum frequency vibrational spectroscopy (SFVS) and second harmonic generation (SHG)) to obtain structural information on polymers. We also studied liquid crystal molecules deposited on polymer surfaces. The first part of the thesis is aimed at understanding liquid crystal (LC) alignment on rubbed polymer surfaces by determining the molecular orientations of LC adsorbates and surface polymer chains. The alignment of LCs by rubbed polymers is not only of fundamental interest but also of practical importance because it is a technique enabling production of

commercial liquid crystal displays. We observed that rubbing induces alignment of surface polymer chains along the rubbing direction, and there is a strong correlation between the molecular orientations of LC adsorbates and the surface chains of rubbed polymers such as polyvinyl alcohol (PVA) and polyimide (6FDA-6CBO). The latter revealed a relatively large but negative pretilt angle, which is highly unusual. On a rubbed polystyrene (PS) surface, we found that the phenyl side groups of PS are oriented perpendicularly to the rubbing direction at the surface, rendering an LC alignment also perpendicular to the rubbing direction.

The second part of the thesis is our discovery of rubbing-induced polar ordering on nylon 11 surfaces. Nylon 11 is known to be ferroelectric. We found that mechanical rubbing can induce strong ferroelectric polarization on an initially amorphous film of nylon 11. The surface chains of rubbed nylon 11 are aligned along the rubbing direction while the induced polarization lies in the surface plane, pointing either to the left or right of the rubbing direction. The probable symmetry breaking process during sample preparation is identified. Based on the experimental results, the surface structure of rubbed nylon 11 appears to be that of a single polar domain.

# Contents

<b>1</b>	<b>Introduction</b>	<b>1</b>
<b>2</b>	<b>Experimental methods</b>	<b>7</b>
2.1	Sum frequency vibrational spectroscopy(SFVS) . . . . .	7
2.2	Second harmonic generation (SHG) . . . . .	12
<b>3</b>	<b>Second harmonic generation study of liquid crystal alignment on a rubbed polyvinyl alcohol surface</b>	<b>16</b>
3.1	Introduction . . . . .	16
3.2	Theoretical background . . . . .	18
3.3	Experiment . . . . .	19
3.4	Results and analysis . . . . .	20
3.5	Discussion . . . . .	22
3.6	Conclusions . . . . .	24
<b>4</b>	<b>Orientations of side chains and adsorbed liquid crystal molecules on a rubbed polyimide surface studied by optical second harmonic generation</b>	<b>25</b>
4.1	Introduction . . . . .	25
4.2	Theoretical background . . . . .	28
4.3	Experiment . . . . .	29
4.4	Results and analysis . . . . .	31
4.5	Discussion . . . . .	38
4.6	Conclusions . . . . .	40
<b>5</b>	<b>Orientations of phenyl sidegroups and liquid crystal molecules on a rubbed polystyrene surface</b>	<b>42</b>
5.1	Introduction . . . . .	42
5.2	Experiment . . . . .	43
5.3	Results, analysis, and discussion . . . . .	44
5.4	Conclusions . . . . .	50

<b>6 Rubbing-Induced Polar Ordering of Nylon 11</b>	<b>51</b>
6.1 Introduction . . . . .	51
6.2 Background . . . . .	53
6.3 Results and analysis . . . . .	53
6.4 Discussion . . . . .	59
6.5 Conclusions . . . . .	61
<b>A Scanning force microscopy on nylon surfaces</b>	<b>62</b>
<b>Bibliography</b>	<b>69</b>

## Acknowledgements

I cannot thank my advisor, Professor Yuen-Ron Shen enough. He dedicated many hours to teaching and guiding me. He taught me not only physics but also how to grow from a student who was just happy to learn things from books and courses to become an independent researcher. He has been a constant source of help, encouragement, and challenge. He was always willing to put his work aside and make himself available to his students and colleagues. Whenever I was stuck on a difficult problem, he helped me find an answer. Through many discussions with him about research problems, I was challenged to get a deeper, clearer, and more complete understanding of physical pictures. I wish to emulate his everlasting curiosity and tireless efforts for correctness and clarity throughout my career.

I would like to thank my fellow graduate students and mentors, Xiaowei Zhuang, Doseok Kim, Paulo Miranda, and Xing Wei. Xiaowei taught me every detail of SHG experiments and how to prepare polymer and liquid crystal samples. Doseok helped me settle down in the beginning of my life in Berkeley. He made me feel like I was with my family. During the experiments with Xing, I learned how to overcome problems and get work done. His humor and cheerfulness will be happily remembered.

I have been fortunate in working with three postdocs in my group, Masahito Oh-e, Chun Zhang, and François Lagurné. The collaboration with Masahito was fruitful. He taught me many practical and up-to-date pieces of knowledge regarding liquid crystals and the fabrication of LCDs. His will to complete his work is remembered as a good resolve to be productive. The time we spent together to fix troubles in our laser is unforgettable.

Chun taught me to use SFVS setups and I was able to get interesting results in my polymer projects with him. François and I started to learn and work on AFM together, and the AFM experiments would have been less fun without him. I would also like to thank all the postdocs and visiting scholars: Kyusang Choi, Joachim Diener, Tomohisa Goto, Wolfgang Beck, Hermann Held, Alexander Lvovsky, Markus Raschke, Karl-Ernst Heinz, Lei Xu, Songhee Han, Zhenlin Wang, Yuh-ling Yeh, and Victor Ostroverkhov.

I would like to wish good luck to the new talented students, John McGuire, Mikhail Belkin, Thai Truong, Na Ji, Luning Zhang, and Weitao Liu. I am obliged to John for proofreading almost all of my manuscripts and publications including this thesis.

I would like to thank Dr. Miquel Salmeron for the opportunity to learn and use his AFM setup and Dr. Monica Luna for teaching me the technique. I would also like to thank Professor S. Z. D. Cheng and Dr. Jason Ge in Akron for providing many interesting materials. I learned that collaboration with good chemists like them is very beneficial.

I would like to acknowledge help from the crew of the machine shop and the electronic shop, especially the help of George Weber, Thomas Pedersen, Joseph Kant, John Davis, and Ron Wyckoff.

I would also like to thank the secretaries in the department and my group: Anne Takizawa, Donna Sakima, Barbara Iwai, Barbara Srulowitz, Anna Engberg, and LaVern Navarro.

I could not have gotten to this moment without my family's support and help. My brothers and sister-in-law, Seok-In, Suklyun, Seokmann, and Bong-Ok, are friends and mentors, who already went through the life of a Ph.D. student and became scientists. Their

enthusiasm and diligence have been an example to me. From them, I learned to appreciate science and nature. They constantly gave me support and encouragement whenever I felt weak and lonely. My nephews, Junrock and Hyunrock, the cutest little guys, always make me smile.

Finally, I would like to thank my parents from the bottom of my heart. They brought me up with unconditional love and care and are the nest I can always return to and rest in. I hope my dad can see from heaven with a smile his youngest son achieve this small accomplishment. This thesis is devoted to my family.

# Chapter 1

## Introduction

In this world, polymers are ubiquitous and indispensable. In life, polymeric materials such as nucleic acids, proteins, and polysaccharides play essential roles in storing and expressing genetic information, building structures, storing energy, and conducting almost all metabolic processes [1]. In modern technology, polymeric materials are extremely useful in achieving desired functions in many applications [2, 3, 4, 5, 6, 7]. Traditionally, polymers have been much loved for their unique combination of advantages such as flexibility, elasticity, plasticity, and ease of fabrication. The incomparable usefulness of polymers becomes more obvious when we realize it is possible to have a seemingly unlimited number of molecular designs and consequently easy to tailor the properties of polymers for desired functions. Recently, new types of polymers such as block co-polymers and dendrimers have opened a new dimension of applications: fabrication of complex nanostructures [8, 9]. Recent advances in polymer science have included the demonstration of metallic conductivity [10], superconductivity [11], electroluminescence [12], rectification [13], ferroelectric-

ity [14, 15], and biocompatibility [16]. Specially treated surfaces of polymers can recognize certain types of molecular materials [17].

The properties of polymers are determined by their structures. The mechanical, electrical, thermal, and optical properties of polymers depend on the chemical and conformational structures of polymers. Polymers made of nonpolar groups such as methylenes tend to be softer and melt at lower temperatures while those containing polar groups tend to be harder and melt at higher temperatures. Polymers with delocalized electrons can be conducting. Linear or branched polymers are thermoplastic, while highly crosslinked ones are thermosetting. Since their discovery more than two decades ago [14], ferroelectric polymers such as poly(vinylidene fluoride) (PVDF) and odd-numbered nylons have drawn much attention due to possible applications in piezoelectric and ultrasonic devices [5]. Odd-numbered nylons like nylon 11 ( $[-\text{NH-CO}-(\text{CH}_2)_{10}-]_n-$ ) have an even number of methylene linkages. The ferroelectricity of such polymers is due to the dipoles associated with certain chemical groups (the amide group in nylons and  $\text{CF}_2$  in PVDF). In nylons, the number of methylene groups is critical in yielding ferroelectricity because even-numbered nylons have their dipoles pointing alternately in opposite directions, which results in no net polarization while odd-numbered ones have their dipoles pointing in the same direction in a single domain, which results in a net polarization (See Fig. 6.1). The pyroelectric, piezoelectric, and ferroelectric properties of nylon 11 have been much studied [15, 18, 19, 20, 21, 22]. In these studies, it was shown the material parameters characterizing these properties of nylon 11 can be comparable to those of ferroelectric crystals such as KDP after thermal and poling treatment. As will be discussed in chapter 6, we have studied ferroelectric ordering

of a thin layer of nylon 11 induced by mechanical rubbing using sum frequency vibrational spectroscopy (SFVS) and second harmonic generation (SHG).

Many applications of polymers rely on the surface properties of polymers, which are determined by their surface structures. The surface structure of a polymer is often different from that of the bulk and needs to be separately characterized. The surface properties of a polymer, such as hydrophobicity or hydrophilicity, depend not only on the chemical structure but also on the molecular conformation of the polymer near the surface. When other molecules are brought into contact with a polymer, their molecular arrangement and ordering on the polymer surface is governed by their interaction with the polymer and therefore influenced by the surface structure of the polymer. Alignment of liquid crystals (LCs) on a rubbed polymer surface is an example that has practical importance in relation to the fabrication of commercial liquid crystal displays (LCDs).

Owing to the growing interest in the surface properties of polymers, many techniques have been developed to study polymer surfaces. Linear optical techniques have often been used but their lack of surface specificity limits their usefulness. Glancing x-ray scattering is capable of determining surface structure on the atomic scale, but it does not have chemical selectivity. Techniques utilizing massive particles require samples under high vacuum; they are not suitable for polymers because polymeric materials often have high vapor pressures or for cases where polymer interfaces with vapors or liquids are of interest. Recently, several novel versatile techniques have been used to probe polymer surfaces or interfaces. Second order nonlinear optical techniques (SFVS and SHG), in particular, have been most successful [23, 24, 25, 26, 27, 28, 29, 30, 31, 32, 33]. NEXAFS (near-edge x-ray ab-

sorption fine structure spectroscopy) is also effective because it has intrinsic surface specificity as well as chemical selectivity [34]. Another useful tool is force microscopy. Even though it does not have chemical selectivity, it can provide useful information about surface topography. Scanning polarization force microscopy (SPFM) and/or kelvin probe microscopy (KPM) allow us to investigate surface polarization separately from surface topography [35].

In the thesis, we demonstrate the possibility of using SHG and SFVS to determine the surface structure of rubbed polymers and molecular adsorbates on them as well as the ferroelectric ordering of nylon 11 induced by rubbing. This thesis is organized as follows. In chapter 2, we will describe the basic theories of the experimental methods we used (nonlinear optical techniques) and how they can yield necessary information for our studies. It will include brief descriptions on the experimental implementation of those methods.

In chapter 3, we will show how we can determine the molecular orientation of an adsorbed liquid crystal monolayer on a rubbed polyvinyl alcohol surface using SHG. Together with SFVS results from a rubbed PVA surface, the alignment of an adsorbed LC monolayer shows a close correlation with that of rubbed PVA chains indicating that the alignment is induced by short-range interactions similar to molecular epitaxy.

In chapter 4, we will show the orientational correlation between the alignment of mesogenic side chains of a polyimide (6FDA-6CBO) and liquid crystal adsorbates using SHG. Since the mesogenic side chains are SHG-active, we could directly probe the orientation of the side chains as well as the LC adsorbates. A LC cell assembled with substrates coated with 6FDA-6CBO shows an interesting negative pretilt angle, which implies that the liquid crystal molecules align anti-parallel to the rubbing direction. This is surprising

because one normally would expect the LC bulk film to assume a parallel alignment. This unusual behavior was understood from the correlated alignment of the polymer side chains and the adsorbed LC molecules at the surface, both of which align anti-parallel to the rubbing direction.

In chapter 5, we study the orientation of phenyl side groups and liquid crystal molecules on a rubbed polystyrene (PS) surface. A rubbed polystyrene surface is known to align a bulk LC film perpendicularly to the rubbing direction when the polymer films are used as the alignment layers for an LC film. We determined the molecular orientation of the phenyl side groups of PS and showed that they are indeed aligned perpendicularly to the rubbing direction. In spite of the weak interaction of LC molecules with the non-polar PS surface, we were able to observe a weak polar anchoring of the LC adsorbates and find an LC alignment correlated with the orientation of the PS side groups, which is perpendicular to the rubbing direction.

In chapter 6, Nylon 11 ( $-\text{[NH-CO-(CH}_2\text{)}_{10}\text{]}_n-$ ) is known to be ferroelectric and consequently has potential applications in piezoelectric devices. We found mechanical rubbing can create strong ferroelectric polarization from amorphous films of nylon 11. SFVS measurements allow us to determine the molecular orientations of all the chemical groups (NH, CO, and CH<sub>2</sub>) in the surface layer of nylon 11 consistently. The chains align along the rubbing direction, and the polarization associated with the amide group lies in the plane of the surface, pointing to either the left or right with respect to the rubbing direction. This lateral polarization could be observed easily with SFVS and SHG measurements. Weak shearing at the surface during sample preparation appears to be responsible for the left-

right symmetry breaking. Our results also indicate that the rubbed surface of nylon 11 is in the form of a single polar domain.

In the Appendix, we summarize the SPFM/KPM study of the surface polarization and prove that the surface polarization of rubbed nylon 11 is planar.

## Chapter 2

# Experimental methods

### 2.1 Sum frequency vibrational spectroscopy(SFVS)

The theory of IR-vis SFVS has been described in detail elsewhere [36, 37]. Sum frequency generation (SFG) is a second order nonlinear optical process. A second order nonlinear polarization is induced by two input fields with the frequencies  $\omega_1$  and  $\omega_2$ . Under the electric dipole approximation, the nonlinear polarization is given by  $\vec{P}(\omega_s) = \epsilon_0 \overset{\leftrightarrow}{\chi}^{(2)}(\omega_s = \omega_1 + \omega_2) : \vec{E}(\omega_1)\vec{E}(\omega_2)$ . For a bulk medium with inversion symmetry, the second order nonlinear susceptibility  $\overset{\leftrightarrow}{\chi}^{(2)}$  should be invariant under inversion but  $\vec{P}(\omega_s)$  and  $\vec{E}(\omega_{1,2})$  change sign. In order for

$$\vec{P}(\omega_s) = \overset{\leftrightarrow}{\chi}^{(2)} : \vec{E}(\omega_1)\vec{E}(\omega_2) \xrightarrow{\text{inversion}} (-\vec{P}(\omega_s)) = \overset{\leftrightarrow}{\chi}^{(2)} : (-\vec{E}(\omega_1))(-\vec{E}(\omega_2)) = \vec{P}(\omega_s) \quad (2.1)$$

to be valid,  $\overset{\leftrightarrow}{\chi}^{(2)}$  should vanish. At the surface or in a medium with no inversion symmetry,  $\overset{\leftrightarrow}{\chi}^{(2)}$  need not be zero, and therefore such a process is allowed. This makes the technique surface-specific and sensitive to polar ordering. The polarization radiates two coherent

beams at frequency  $\omega_s$  in the reflection and transmission directions. The output angle of the SF beam is given by wavevector matching in the plane of the surface:  $k_{1,\parallel} + k_{2,\parallel} = k_{s,\parallel}$ , where  $k_{i,\parallel}$  is the horizontal component of the wavevector  $\vec{k}_i$ . With  $\vec{P}(\omega_s)$  given, one can solve the wave equation and obtain the SF output intensity

$$I(\omega_s) = \frac{\omega_s^2 \sec^2 \beta_s}{8\epsilon_0 c^3} |\chi_{\text{EFF}}^S|^2 I(\omega_1) I(\omega_2), \quad (2.2)$$

where  $\chi_{\text{EFF}}^S = (\vec{L}(\omega_s) \cdot \hat{e}(\omega_s)) \cdot \overleftrightarrow{\chi}_{\text{S,eff}}^{(2)} \cdot (\vec{L}(\omega_1) \cdot \hat{e}(\omega_1)) (\vec{L}(\omega_2) \cdot \hat{e}(\omega_2))$ ,  $\beta_i$  is the incidence angle of the beam at  $\omega_i$ ,  $\hat{e}(\omega_i)$  the unit polarization vector,  $\vec{L}(\omega_i)$  the macroscopic local field correction tensor, and  $I(\omega_i)$  the beam intensity.  $\overleftrightarrow{\chi}_{\text{S,eff}}^{(2)}$  is given by

$$\overleftrightarrow{\chi}_{\text{S,eff}}^{(2)} = \overleftrightarrow{\chi}_{\text{S}}^{(2)} + \frac{\overleftrightarrow{\chi}_{\text{B}}^{(2)}}{k_{s,z} - k_{1,z} - k_{2,z}}, \quad (2.3)$$

which contains contributions from the surface and the bulk represented by the surface and bulk susceptibilities  $\overleftrightarrow{\chi}_{\text{S}}^{(2)}$  and  $\overleftrightarrow{\chi}_{\text{B}}^{(2)}$ , respectively. The factor  $l_{\text{coh}} = \frac{1}{k_{s,z} - k_{1,z} - k_{2,z}}$  is usually defined as the coherence length. Note that  $k_{s,z}$  will have opposite signs for the reflected and transmitted SF signals, and therefore  $l_{\text{coh}}$  is very different for the two geometries. In general,  $\overleftrightarrow{\chi}_{\text{S,eff}}^{(2)}$  has 27 independent elements. However, we can use the symmetry of the system to reduce the number of nonvanishing independent elements. In the case of an azimuthally isotropic interface, there are only 4 independent nonvanishing elements. With the laboratory coordinates chosen such that  $\hat{z}$  is along the surface normal and  $\hat{x}$  in the incidence plane, (with subscripts S, eff omitted) they are

$$\chi_{xxz}^{(2)} = \chi_{yyz}^{(2)}, \quad \chi_{xzx}^{(2)} = \chi_{yzy}^{(2)}, \quad \chi_{zxx}^{(2)} = \chi_{zyy}^{(2)}, \quad \chi_{zzz}^{(2)}. \quad (2.4)$$

These four elements can be deduced by measuring SF signal with the four input and output polarization combinations that are not required by symmetry to be zero, namely SSP (refer-

ring to S-polarized SF field, S-polarized  $\vec{E}(\omega_1)$ , and P-polarized  $\vec{E}(\omega_2)$ , respectively), SPS, PSS, and PPP. The effective nonlinear susceptibility for the four polarization combinations can be expressed as

$$\begin{aligned}
\chi_{\text{EFF,SSP}}^{\text{S}} &= L_{yy}(\omega_s)L_{yy}(\omega_1)L_{zz}(\omega_2) \sin\beta_2 \chi_{yyz}^{(2)}, \\
\chi_{\text{EFF,SPS}}^{\text{S}} &= L_{yy}(\omega_s)L_{zz}(\omega_1)L_{yy}(\omega_2) \sin\beta_1 \chi_{yzy}^{(2)}, \\
\chi_{\text{EFF,PSS}}^{\text{S}} &= L_{zz}(\omega_s)L_{yy}(\omega_1)L_{yy}(\omega_2) \sin\beta_s \chi_{zyy}^{(2)}, \\
\chi_{\text{EFF,PPP}}^{\text{S}} &= L_{zz}(\omega_s)L_{zz}(\omega_1)L_{zz}(\omega_2) \sin\beta_s \sin\beta_1 \sin\beta_2 \chi_{zzz}^{(2)} \\
&\quad - L_{xx}(\omega_s)L_{xx}(\omega_1)L_{zz}(\omega_2) \cos\beta_s \cos\beta_1 \sin\beta_2 \chi_{xzx}^{(2)} \\
&\quad - L_{xx}(\omega_s)L_{zz}(\omega_1)L_{xx}(\omega_2) \cos\beta_s \sin\beta_1 \cos\beta_2 \chi_{zxx}^{(2)} \\
&\quad + L_{zz}(\omega_s)L_{xx}(\omega_1)L_{xx}(\omega_2) \sin\beta_s \cos\beta_1 \cos\beta_2 \chi_{zxx}^{(2)}.
\end{aligned}$$

$L_{xx}(\omega)$ ,  $L_{yy}(\omega)$ , and  $L_{zz}(\omega)$  are the diagonal elements of  $\overleftrightarrow{L}(\Omega)$  given at the interface between media 1 and 2 by

$$\begin{aligned}
L_{xx}(\omega) &= \frac{2 n_1(\omega) \cos \gamma}{n_1(\omega) \cos \gamma + n_2(\omega) \cos \beta}, \\
L_{yy}(\omega) &= \frac{2 n_1(\omega) \cos \beta}{n_1(\omega) \cos \beta + n_2(\omega) \cos \gamma}, \\
L_{zz}(\omega) &= \frac{2 n_2(\omega) \cos \beta}{n_1(\omega) \cos \gamma + n_2(\omega) \cos \beta} \left( \frac{n_1(\omega)}{n'(\omega)} \right)^2
\end{aligned} \tag{2.5}$$

where  $n'(\omega)$  is the refractive index of the interfacial layer and  $\gamma$  the angle of the beam in the sample. In chapter 6,  $n'(\omega)$  is the refractive index of nylon 11 film because the SF signal is mainly from the bulk film. More nonvanishing tensor elements exist for an anisotropic surface. By measuring  $|\chi_{\text{EFF}}^{\text{S}}|$ , which is a linear combination of the nonlinear susceptibility tensor elements, for various polarization combinations and sample orientations, we can determine all nonvanishing tensor elements. Since  $\chi^{\leftrightarrow(2)}$  is resonantly enhanced when  $\omega_2$

approaches a vibrational resonance, scanning over such resonances yields an SF vibrational spectrum. We can express  $\overleftrightarrow{\chi}^{(2)}$  in terms of the resonant nonlinear polarizability  $\overleftrightarrow{\alpha}_R^{(2)}$  for the molecular groups,

$$\overleftrightarrow{\chi}^{(2)} = \overleftrightarrow{\chi}_{NR}^{(2)} + N \int \overleftrightarrow{\alpha}_R^{(2)}(\Omega) f(\Omega) d\Omega \quad (2.6)$$

where  $\overleftrightarrow{\chi}_{NR}^{(2)}$  describes the nonresonant contribution,  $N$  is the number density of molecules,  $\Omega$  denotes a set of orientational angles  $(\theta, \phi, \psi)$ , and  $f(\Omega)$  is the orientational distribution function. We assume that  $\overleftrightarrow{\alpha}_R^{(2)}$  is composed of Lorentzian resonant terms,

$$\overleftrightarrow{\alpha}_R^{(2)} = \sum_q \frac{\overleftrightarrow{a}_q^{(2)}}{\omega_2 - \omega_q + i\Gamma_q} \quad (2.7)$$

where  $\overleftrightarrow{a}_q^{(2)}$ ,  $\omega_q$ , and  $\Gamma_q$  are the amplitude, resonant frequency, and damping constant, respectively, of the  $q^{\text{th}}$  molecular vibrational mode. Insertion of Eq. 2.7 into Eq. 2.6 gives

$$\begin{aligned} \overleftrightarrow{\chi}^{(2)} &= \overleftrightarrow{\chi}_{NR}^{(2)} + \sum_q \frac{\overleftrightarrow{A}_q}{\omega_2 - \omega_q + i\Gamma_q} \\ \overleftrightarrow{A}_q &= N \int \overleftrightarrow{a}_q^{(2)}(\Omega) f(\Omega) d\Omega. \end{aligned} \quad (2.8)$$

From the observed dispersion of  $\overleftrightarrow{\chi}^{(2)}$ , we can deduce  $\overleftrightarrow{A}_q$  in Eq. 2.8. We can also obtain  $\overleftrightarrow{a}_q^{(2)}$  from other measurements or theoretical calculations and models. Then, the second equation of Eq. 2.8 enables us to obtain an approximate orientational distribution function  $f(\Omega)$  that assumes a certain functional form.

In our experiments, the SFVS setup consists of a pulsed laser system that generates a tunable IR pulse and a fixed frequency ‘visible’ pulse. The ‘visible’ beam could be 532 nm or 1064 nm. The pulses are temporally and spatially overlapped at the sample surface and the SF signal is detected by a photomultiplier(PMT)/gated integrator detection system

or a liquid-nitrogen-cooled CCD camera after spatial and spectral filtering to eliminate fluorescence and stray light. A schematic diagram of our SFVS setup is shown in Fig. 2.1 and 2.2. For the work reported in this thesis, two SFVS setups were used. Most of the data in chapter 6 were taken with an old setup (setup A), while the data in chapter 5 and the CO spectra in chapter 6 were taken with a newer setup (setup B). In setup A, the main laser source is a homebuilt high power Nd:YAG laser with wavelength  $1.06 \mu\text{m}$ , 10 mJ pulse energy, and  $\sim 40$  ps pulsewidth, operating at a repetition rate of 10 Hz. The infrared generation is from an optical parametric generator and amplifier (OPG/OPA) based on two  $\text{LiNbO}_3$  crystals. It generates pulses with energy of  $\sim 200 \mu\text{J}$  and pulsewidth of  $\sim 20$  ps and is tunable from  $2.5$  to  $4 \mu\text{m}$  ( $4000$  to  $2500 \text{ cm}^{-1}$ ) [38, 39]. The visible and IR pulses are incident on the sample at angles of  $39^\circ$  and  $51^\circ$  relative to the surface normal in a counter-propagating scheme and have spot sizes of approximately  $300 \mu\text{m}$  and  $500 \mu\text{m}$ , respectively.

In setup B, the main laser source is a commercial high-power Nd:YAG laser with  $\lambda = 1.06 \mu\text{m}$ , 30 mJ pulse energy and  $\sim 25$  ps pulsewidth, operating at a repetition rate of 20 Hz. The infrared generation is achieved in a  $\text{AgGaS}_2$  crystal by difference frequency generation (DFG) using part of the  $1.06 \mu\text{m}$  laser beam and tunable near-IR radiation from an OPG/OPA system as inputs. This system has been described in detail elsewhere [39, 40] and is shown schematically in Fig 2.2. The DFG stage generates IR pulses of energy  $\sim 100 \mu\text{J}$  and pulsewidth  $\sim 15$  ps, tunable from  $2.5 \mu\text{m}$  to  $9 \mu\text{m}$  ( $4000 \sim 1100 \text{ cm}^{-1}$ ) with  $6 \text{ cm}^{-1}$  bandwidth. The visible pulses at  $532 \text{ nm}$  are generated by SHG in a BBO crystal and have an energy of about 1.5 mJ and pulsewidth  $\sim 18$  ps. In this setup, there are two separate

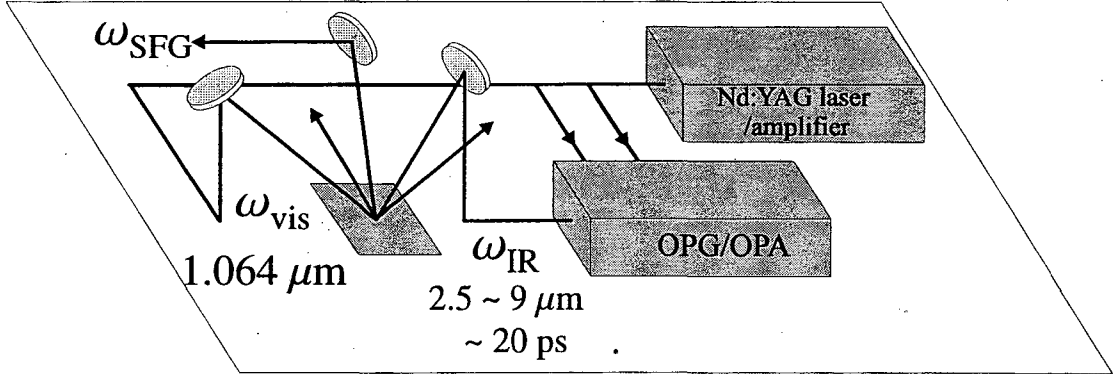


Figure 2.1: Schematic diagram of a SFVS setup (setup A and the second arm of setup B)

measurement arms. In the first arm, the 532 nm visible and IR pulses are incident on the sample at angles  $45^\circ$  and  $57^\circ$ , respectively, in a co-propagating scheme. The SF detection system is similar to the one in setup A. In the second arm, the inputs are incident on the sample in a counter-propagating scheme, and the detection system is a nitrogen-cooled CCD camera. The details on the second arm can be found in Ref. [39].

## 2.2 Second harmonic generation (SHG)

The theory for surface SHG has been described in detail elsewhere [41, 42]. SHG is also a second-order nonlinear optical process and surface-specific. In the process, a nonlinear optical polarization  $\vec{P}(2\omega)$  is induced by the input optical field  $\vec{E}(\omega)$ . In the electric dipole approximation,  $\vec{P}(2\omega) = \overset{\leftrightarrow}{\chi}^{(2)} : \vec{E}(\omega)\vec{E}(\omega)$ . The SHG intensity from the surface into the reflection direction is given by Eq. 2.2 by setting  $\omega_s = 2\omega$  and  $\omega_1 = \omega_2 = \omega$  and using

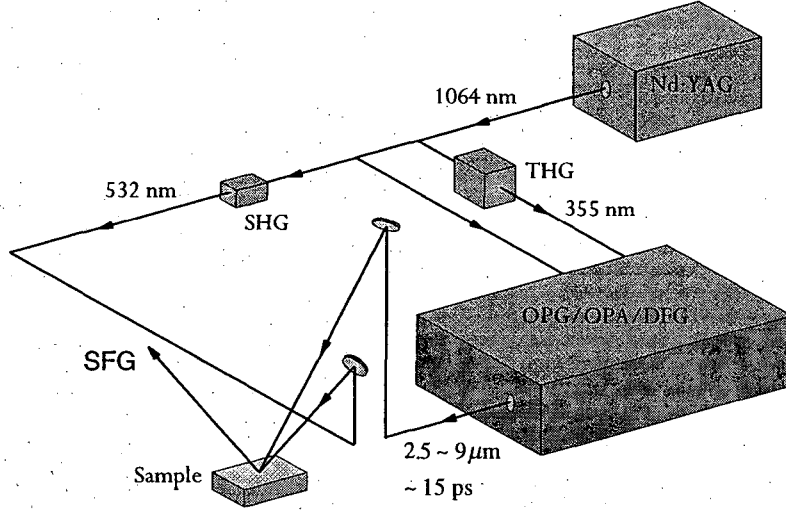


Figure 2.2: Schematic diagram of a SFVS setup (the first arm of setup B)

appropriate  $\vec{L}(\Omega)$ . For  $\vec{L}(\Omega)$  for the thin-film system that represents the polymer-coated substrates, see Appendix A in Ref. [43].

Our interest is to determine the molecular orientation from the SHG measurement using various polarization combinations and sample orientations. The nonlinear susceptibility  $\chi_{ijk}^{(2)}$  is given by

$$\chi_{ijk}^{(2)} = N \langle (\hat{\xi} \cdot \hat{i})(\hat{\eta} \cdot \hat{j})(\hat{\zeta} \cdot \hat{k}) \rangle \alpha_{\xi\eta\zeta}^{(2)} \quad (2.9)$$

where  $N$  is the number density of molecules. If the molecules are rod-like so that  $\alpha^{(2)}$  is dominated by a single element  $\alpha_{\xi\xi\xi}^{(2)}$ , with  $\hat{\xi}$  being the unit vector along the long molecular axis,

$$\chi_{ijk}^{(2)} = N \langle (\hat{\xi} \cdot \hat{i})(\hat{\xi} \cdot \hat{j})(\hat{\xi} \cdot \hat{k}) \rangle \alpha_{\xi\xi\xi}^{(2)} \quad (2.10)$$

where  $\hat{i}$ ,  $\hat{j}$ , and  $\hat{k}$  are unit vectors in the laboratory coordinates. In the case that the orientation of the molecules is azimuthally isotropic, the nonlinear susceptibility tensor has

only two nonvanishing elements:

$$\begin{aligned}\chi_{zzz}^{(2)} &= N\alpha_{\xi\xi\xi}^{(2)} \langle \cos^3\theta \rangle \\ \chi_{zxx}^{(2)} = \chi_{xzx}^{(2)} = \chi_{xxz}^{(2)} = \chi_{zyy}^{(2)} = \chi_{yzy}^{(2)} = \chi_{yyz}^{(2)} &= \frac{1}{2}N\alpha_{\xi\xi\xi}^{(2)} \langle \cos\theta \sin^2\theta \rangle\end{aligned}$$

where  $\theta$  is the angle between the surface normal  $\hat{z}$  and the molecular long axis  $\hat{\xi}$  as shown in the inset of Fig. 4.2. By measuring SHG with the polarization combinations  $S_{\text{in}}P_{\text{out}}$  and  $P_{\text{in}}P_{\text{out}}$ , where subscripts indicate the field for which the polarization is defined, we can determine  $\chi_{zzz}^{(2)}$  and  $\chi_{zxx}^{(2)}$ . When the surface has  $C_{1v}$  symmetry with the mirror plane along the  $x$  direction,  $\chi^{\leftrightarrow(2)}$  has six nonvanishing independent elements:

$$\begin{aligned}\chi_{zzz}^{(2)} &= N\alpha_{\xi\xi\xi}^{(2)} \langle \cos^3\theta \rangle, \\ \chi_{zxx}^{(2)} &= \chi_{xzx}^{(2)} = \chi_{xxz}^{(2)} = N\alpha_{\xi\xi\xi}^{(2)} \langle \sin^2\theta \cos\theta \cos^2\phi \rangle, \\ \chi_{zyy}^{(2)} &= \chi_{yzy}^{(2)} = \chi_{yyz}^{(2)} = N\alpha_{\xi\xi\xi}^{(2)} \langle \sin^2\theta \cos\theta \sin^2\phi \rangle, \\ \chi_{xxx}^{(2)} &= N\alpha_{\xi\xi\xi}^{(2)} \langle \sin^3\theta \cos^3\phi \rangle, \\ \chi_{xzz}^{(2)} &= \chi_{zxx}^{(2)} = \chi_{zzx}^{(2)} = N\alpha_{\xi\xi\xi}^{(2)} \langle \sin\theta \cos^2\theta \cos\phi \rangle, \\ \chi_{xyy}^{(2)} &= \chi_{yxy}^{(2)} = \chi_{yyx}^{(2)} = N\alpha_{\xi\xi\xi}^{(2)} \langle \sin^3\theta \sin^2\phi \cos\phi \rangle\end{aligned}\tag{2.11}$$

where  $\theta$  and  $\phi$  are the polar and azimuthal angles of  $\hat{\xi}$  in the  $xyz$  plane (See Fig. 4.2). We can determine these six elements using four different polarization combinations ( $S_{\text{in}}S_{\text{out}}$ ,  $S_{\text{in}}P_{\text{out}}$ ,  $P_{\text{in}}P_{\text{out}}$ , and  $P_{\text{in}}S_{\text{out}}$ ) together with various sample orientations. From the measured  $\chi_{ijk}^{(2)}$ , assuming a molecular distribution function of the form

$$g(\theta, \phi) = A \exp\left[-\frac{(\theta - \theta_0)^2}{2\sigma^2}\right] \times (1 + d_1 \cos\phi + d_2 \cos 2\phi + d_3 \cos 3\phi),\tag{2.12}$$

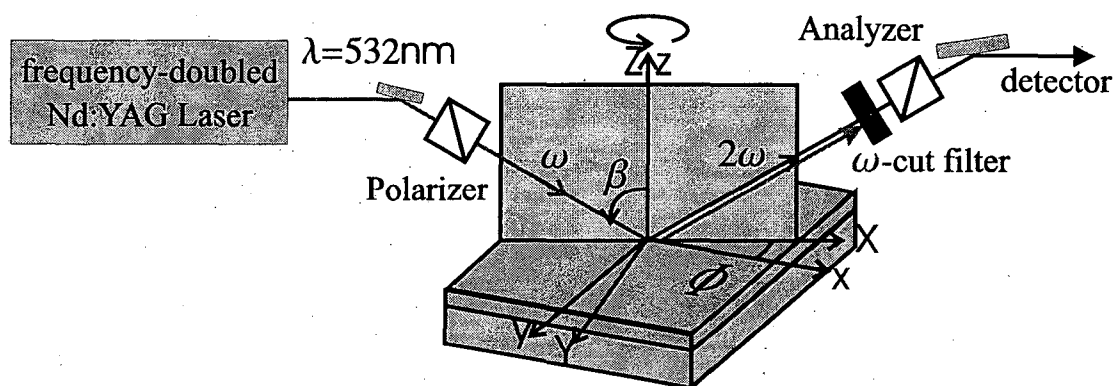


Figure 2.3: Schematic diagram of SHG setup

we can determine the coefficients  $\theta_0$ ,  $\sigma$ ,  $d_1$ ,  $d_2$ , and  $d_3$  that define the distribution. The experimental setup for SHG is shown in Fig 2.3. The source is a frequency doubled Q-switch mode-locked Nd:YAG laser. The fundamental wavelength, the repetition rate, the pulsewidth, and the incidence angle  $\beta$  are 532 nm, 500 Hz,  $\sim 150$  ns, and  $67^\circ$ , respectively. The SHG signal is highly coherent and directional. Using spectral filtering, the SHG in the reflection direction can be detected by a PMT and gated electronics.

## Chapter 3

# Second harmonic generation study of liquid crystal alignment on a rubbed polyvinyl alcohol surface

### 3.1 Introduction

The alignment of liquid crystal (LC) molecules on rubbed polymer surfaces was discovered in 1911 [44]. In recent years, this phenomenon has been studied extensively not only because of the basic interest in understanding the underlying mechanism but also because of its relevance to LC display technology. Today, rubbed polymer films are widely used in industry to obtain homogeneous bulk LC alignment for LC displays [45]. Different mechanisms have been proposed for LC alignment on rubbed polymer surfaces. One assumes that rubbing creates microgrooves or scratches on polymer surfaces which then align the LC along the

grooves to minimize the energy of elastic distortion [46]. Another suggests that rubbing aligns surface polymer chains which in turn align the LC through intermolecular interaction [47]. The latter is believed to be operative when LC molecules anchor strongly to polymer surfaces, as is commonly the case in the LC industry.

To study LC alignment by rubbed polymer surfaces, a number of experimental techniques have been used. Atomic force microscopy (AFM) can provide images of rubbed polymer surfaces showing an overall anisotropy but is unable to resolve the surface polymer chains [48, 49, 50]. Ellipsometry [51] and infrared spectroscopy [52, 53, 54, 55] can measure rubbing-induced anisotropy and other structural changes in the polymer film. However, because of their lack of surface specificity, it is unclear whether these results indeed represent the real surface structure of the rubbed polymer. Glancing incidence x-ray scattering (GIXS) can probe a surface region of  $\sim 5$  nm thick [56, 57]. A higher surface sensitivity has been achieved by near-edge x-ray absorption fine structure (NEXAFS) spectroscopy, which can probe a surface layer of  $\sim 1$  nm thick [34].

SHG is an ideal tool to study interfacial structure between two centro-symmetric media. Being a second order nonlinear optical process, SHG is surface-specific and monolayer-sensitive. In this work, optical SHG showed that an adsorbed LC monolayer (4'-*n*-octyl-4-cyanobiphenyl: 8CB) is well aligned along the rubbing direction and that the molecular alignment of the monolayer has a strong correlation with that of a rubbed PVA surface that was thoroughly studied by sum frequency generation spectroscopy [26]. SHG studies of LC alignment on rubbed polymers have also been conducted by others [43, 58].

### 3.2 Theoretical background

The theory of surface SHG has been described in detail in chapter 2 and elsewhere [41, 43]. Surface SHG is generated in reflection from a surface nonlinear polarization  $\vec{P}^{(2)}(2\omega)$  induced at an interface by the input field  $\vec{E}(\omega)$ , and the output intensity is given by

$$\begin{aligned}
 I(2\omega) &\propto |(\hat{e}(2\omega) \cdot \vec{L}(2\omega)) \cdot \vec{P}^{(2)}(2\omega)|^2 \\
 &\propto |(\hat{e}(2\omega) \cdot \vec{L}(2\omega)) \overset{\leftrightarrow}{\chi}^{(2)} : (\vec{L}(\omega) \cdot \hat{e}(\omega))(\vec{L}(\omega) \cdot \hat{e}(\omega))|^2 |\vec{E}(\omega)|^4 \\
 &\equiv |\chi_{\text{EFF}}^S(\Phi)|^2 |\vec{E}(\omega)|^4
 \end{aligned} \tag{3.1}$$

where  $\hat{e}(\Omega)$  is the unit polarization vector,  $\vec{L}(\Omega)$  is the Fresnel factor at frequency  $\Omega$ , and  $\Phi$  defines the azimuthal orientation of the sample in the laboratory coordinates.  $\overset{\leftrightarrow}{\chi}^{(2)}$  is the surface nonlinear susceptibility tensor, and  $\chi_{\text{EFF}}^S$ , as defined, depends on  $\Phi$  through  $\hat{e}(\Omega)$  with respect to the sample orientation. SHG measurements with different sample orientations allow us to determine  $\chi_{\text{EFF}}^S(\Phi)$  for four different polarization combinations ( $S_{\text{in}}S_{\text{out}}$ ,  $S_{\text{in}}P_{\text{out}}$ ,  $P_{\text{in}}S_{\text{out}}$ , and  $P_{\text{in}}P_{\text{out}}$ ). The relation between  $\chi_{\text{EFF}}^S(\Phi)$  and  $\overset{\leftrightarrow}{\chi}^{(2)}$ , which is given explicitly in Eq.(7) of Ref. [43], then permits the deduction of all the nonvanishing  $\chi_{ijk}^{(2)}$  elements.

For 4'-*n*-octyl-4 cyanobiphenyl (8CB) as a rod-like molecule,  $\chi_{ijk}^{(2)}$  can be expressed by Eq. 2.10. For a monolayer of 8CB on a rubbed polymer surface with  $C_{1v}$  symmetry, the nonvanishing  $\chi_{ijk}^{(2)}$  elements and the molecular distribution of the 8CB molecule at the surface,  $g(\theta, \phi)$ , are described by Eqs. 2.11 and 2.12, respectively. The five parameters in  $g(\theta, \phi)$  of Eq. 2.12 provide an approximate orientational distribution of the adsorbed 8CB molecules.

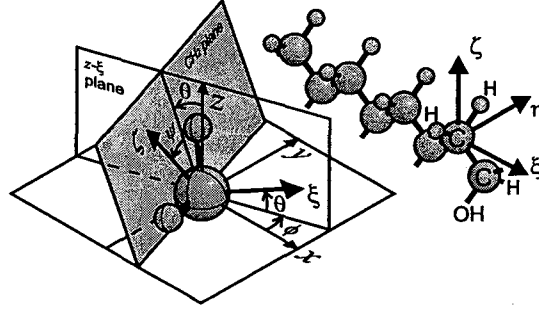


Figure 3.1: Molecular structure of PVA and orientational geometry of a  $\text{CH}_2$  group on a rubbed PVA surface.  $\hat{x}$  is along the rubbing direction, and  $\hat{z}$  is along the surface normal of the polymer film.

### 3.3 Experiment

Polyvinyl alcohol (PVA:  $[-\text{CH}_2-\text{HC}(\text{OH})-]_n$ ) (Scientific Polymer Products, Inc., M.W. = 14,000, 100 % hydrolyzed) was dissolved in water (1.5 wt. %) at  $100^\circ\text{C}$  for 1 hour, spin-coated (3000 rpm, 30 sec.) on fused quartz plates, baked at  $100^\circ\text{C}$  for 1 hour, and rubbed once with a velvet cloth. The film thickness was about 30 nm, and the rubbing strength used was at a saturation level. 8CB was deposited onto rubbed PVA by thermal evaporation using an oven temperature of  $60^\circ\text{C}$ . SHG was used to monitor the deposition of 8CB on the substrate in situ. Formation of a monolayer is indicated by the leveling of the SHG signal [59]. The sample was mounted on a  $360^\circ$  rotational stage and SHG signal was measured for every  $10^\circ$  increment of the azimuthal angle from  $0^\circ$  to  $350^\circ$ . The resultant  $|\chi_{\text{EFF}}^S(\Phi)|$  then allowed us to deduce  $\chi_{ijk}^{(2)}$  accurately. We collected SHG data for four different input/output polarization combinations:  $S_{\text{in}}S_{\text{out}}$ ,  $S_{\text{in}}P_{\text{out}}$ ,  $P_{\text{in}}S_{\text{out}}$ , and  $P_{\text{in}}P_{\text{out}}$ .

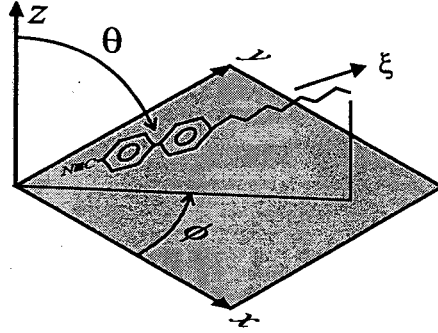


Figure 3.2: Molecular structure and orientational coordinates of an 8CB molecule deposited on a rubbed PVA surface.  $\hat{\xi}$  is along the long axis of the cyanobiphenyl core of the 8CB molecule.  $\theta$  and  $\phi$  are the polar and azimuthal angles of  $\hat{\xi}$ . The  $x$  axis stands for the rubbing direction.

### 3.4 Results and analysis

We present in Fig. 3.3 the SHG intensities from the 8CB monolayer on a rubbed PVA surface as a function of the sample azimuthal angle  $\Phi$  for different input/output polarization combinations.

The six nonvanishing independent  $\chi_{ijk}^{(2)}$  elements can be deduced by fitting the data in Fig. 3.3 using Eq. (3.1) and Eq. 7 in Ref. [43]. The fits are plotted as solid lines in Fig. 3.3, and the deduced nonvanishing  $\chi_{ijk}^{(2)}$  elements are presented in Table 3.1.

We determined the five parameters needed to fit the orientational distribution function in Eq. 2.12 to the data. The results are presented in Table 3.2. In this case,  $\epsilon'$  cannot be determined separately, and the assumption  $\epsilon'(\omega)=\epsilon'(2\omega)$  used here also may not be true because of the electronic resonance of 8CB molecules at the second-harmonic frequency. Nevertheless, as shown in Table 3.2, varying  $\epsilon'$  from 1 to 2.25 mainly changes

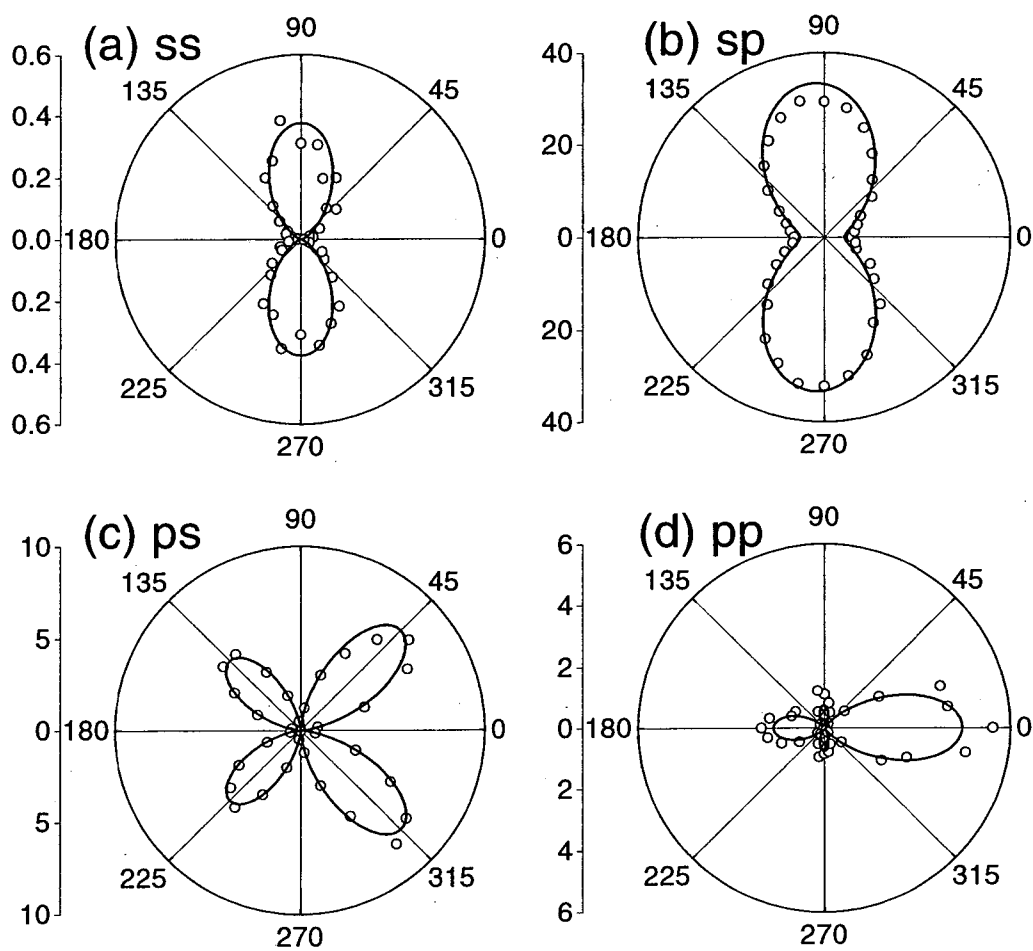


Figure 3.3: Polar plots of SHG intensities (arbitrary units) from an 8CB monolayer on a rubbed PVA surface.  $0^\circ$  and  $180^\circ$  are the rubbing and anti-rubbing directions, respectively. Circles are the experimental data and solid lines are the theoretical fits. The input-output polarization combinations are (a)  $S_{in}S_{out}$ , (b)  $S_{in}P_{out}$ , (c)  $P_{in}S_{out}$ , and (d)  $P_{in}P_{out}$ .

Table 3.1: Nonvanishing independent  $\chi_{ijk}^{(2)}$  elements of the 8CB monolayer on rubbed PVA deduced from the SHG experiment with the  $zzz$  component normalized to 1.

$\chi_{zzz}^{(2)}/\epsilon'^3$	1
$\chi_{xxx}^{(2)}$	$3.0 \pm 0.5$
$\chi_{xyy}^{(2)}$	$0.32 \pm 0.25$
$\chi_{xzz}^{(2)}/\epsilon'^2$	$0.15 \pm 0.09$
$\chi_{zxx}/\epsilon'$	$11.5 \pm 0.8$
$\chi_{zyy}/\epsilon'$	$4.4 \pm 0.4$

Table 3.2: Deduced parameters in  $g(\theta, \phi)$  for various values of the surface dielectric constant  $\epsilon'$  of the 8CB monolayer.

$\epsilon'$	$\theta_0$ (deg.)	$\sigma$ (deg.)	$d_1$	$d_2$	$d_3$
1.0	$80 \pm 5$	$6 \pm 3$	$.07 \pm .03$	$.85 \pm .03$	$.04 \pm .02$
1.25	$78 \pm 6$	$8 \pm 4$	$.07 \pm .03$	$.85 \pm .03$	$.04 \pm .02$
1.5	$75 \pm 8$	$9 \pm 4$	$.07 \pm .03$	$.85 \pm .03$	$.04 \pm .02$
1.75	$72 \pm 9$	$10 \pm 5$	$.07 \pm .03$	$.85 \pm .03$	$.04 \pm .02$
2.0	$69 \pm 10$	$11 \pm 5$	$.07 \pm .03$	$.85 \pm .03$	$.04 \pm .02$
2.25	$66 \pm 12$	$12 \pm 6$	$.07 \pm .03$	$.85 \pm .03$	$.04 \pm .02$

the deduced values of  $\theta$  and  $\sigma$ , and has little effect on the parameters  $d_1$ ,  $d_2$ , and  $d_3$  which describe the azimuthal distribution.

### 3.5 Discussion

From the SHG and SFVS [26] studies, we have obtained the orientational distribution functions  $f(\tilde{\theta}, \tilde{\phi}, \tilde{\psi}) = C e^{-\frac{(\tilde{\theta}-\tilde{\theta}_0)^2}{2\sigma_\theta^2} - \frac{(\tilde{\phi}-\tilde{\phi}_0)^2}{2\sigma_\phi^2} - \frac{(\tilde{\psi}-\tilde{\psi}_0)^2}{2\sigma_\psi^2}}$  for the surface PVA chains ( $C$  is a normalization constant) and  $g(\theta, \phi)$  for the molecules in the 8CB monolayer independently. It is important to determine the correlation between them. In order to do so, we calculate a grand azimuthal distribution function  $F(\tilde{\phi})$  for PVA chains by integrating  $f(\tilde{\theta}, \tilde{\phi}, \tilde{\psi})$  over  $\tilde{\theta}$  and  $\tilde{\psi}$ , and also  $G(\phi)$  for the 8CB molecules by integrating  $g(\theta, \phi)$  over  $\theta$ . However, we

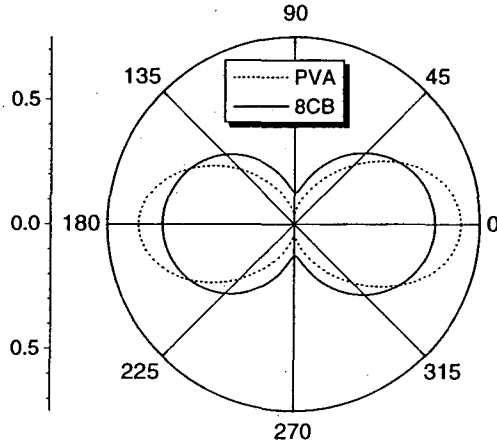


Figure 3.4: Polar plot of the grand azimuthal distribution functions of the PVA chains (dashed line) and 8CB molecules (solid line) on a rubbed PVA surface. Square root values are used so that the total areas inside the two curves remain constant.

notice that unlike an 8CB molecule, a section of PVA chain has no polarity, i.e.,  $(\tilde{\theta}, \tilde{\phi})$  and  $(-\tilde{\theta}, \tilde{\phi} + 180^\circ)$  describe the same chain orientation. To define  $f(\tilde{\theta}, \tilde{\phi}, \tilde{\psi})$  over all orientations, we can limit  $\tilde{\theta}$  between  $0^\circ$  and  $90^\circ$  and vary  $\tilde{\phi}$  over the entire  $360^\circ$ . We naturally use the same limiting ranges for  $\theta$  and  $\phi$  to define  $g(\theta, \phi)$  for polar 8CB molecules. A polar plot of  $\sqrt{F(\tilde{\phi})}$  and  $\sqrt{G(\phi)}$  are presented in Fig. 3.4. The correlation between the two is remarkable. As expected, the polymer chains on the rubbed PVA surface appear to be more ordered in the azimuthal distribution than the adsorbed 8CB monolayer. This suggests that the rubbed polymer surface indeed serves as a molecular template to align LC molecules through short-range molecular interactions [60]. The forward/backward asymmetry of the 8CB orientational distribution (represented by the positive coefficient  $d_1 = 0.07$ ) indicates that the 8CB molecules prefer to align in the forward direction. This must be somehow related to the average upward tilt angle ( $\tilde{\theta}_0 = 2.5^\circ$ ) of the PVA chains [26]. Similar results have also been found for other rubbed polymers [34, 54], yet no theoretical model is avail-

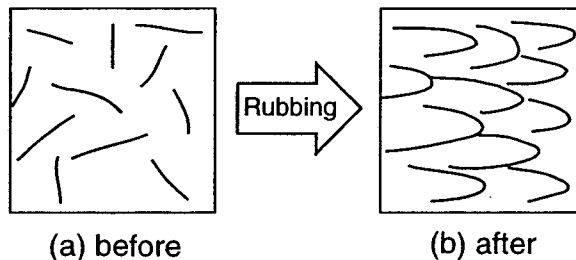


Figure 3.5: Proposed polymer chain distribution (top view) on a PVA surface (a) before and (b) after rubbing.

able to correlate these two tilt angles quantitatively. There are, however, some qualitative explanations. For example, it has been assumed that rubbing induces a saw-tooth-like polymer surface which leads to a homogeneous LC alignment with a forward pretilt angle [61]. This is consistent with the scenario we proposed for the rubbed PVA surface (Fig. 3.5), in which the 8CB molecules adsorbed on the back-slanted terraces would appear to align more in the forward direction. As demonstrated in Ref [58], the LC monolayer then governs the forward pretilt angle of a bulk LC film.

### 3.6 Conclusions

We have used SHG to determine the orientational distribution of a monolayer of 8CB molecules adsorbed on a rubbed PVA surface, the orientational distribution of which was determined with SFVS. Comparison of the two in the azimuthal plane shows that they are well correlated. This strongly supports the claim that “orientational epitaxy” is the mechanism responsible for the surface-induced LC bulk alignment by rubbed polymer surfaces. We have proposed a possible scenario for how rubbing changes the polymer chain conformation at the surface.

## Chapter 4

# Orientations of side chains and adsorbed liquid crystal molecules on a rubbed polyimide surface studied by optical second harmonic generation

### 4.1 Introduction

Understanding liquid crystal (LC) alignment on mechanically rubbed surfaces is of great practical importance for the design of LC displays (LCDs). The problem has been studied extensively in the past [23, 26, 34, 43, 47, 58, 62, 63]. It is believed that rubbing aligns

the surface polymer chains, which in turn align the LC layer adsorbed on the surface [47]. Recently, x-ray spectroscopy was used to measure quantitatively the alignment of surface polymer chains [34]. With sum-frequency vibrational spectroscopy and optical second harmonic generation, Wei *et al.* were able to obtain the orientational distributions of the surface polymer chains and the adsorbed LC monolayer and show that the two are well correlated [26]. However, details of LC alignment on different types of rubbed polymers are still not well understood.

One of the important design parameters for LCDs is the pretilt angle of LC alignment in a film. To achieve a reasonable gray scale for LCDs, a sufficiently large pretilt angle is needed. For example, for LCDs in the super-twist-nematic operation mode, a pretilt as large as  $\sim 15^\circ$  is desired [64]. How to make an LC cell with a large pretilt has been a subject of immense interest to many researchers. Polymers with appropriate side chains appear to be a viable solution. While rubbing aligns the LC homogeneously, the side chains may help induce a large LC tilt angle. One such polymer is 6FDA-6CBO (This polymer is synthesized by a one-step polymerization method from 2,2'-bis(3,4-dicarboxyphenyl)hexafluoropropane dianhydride (6FDA) and 2,2'-bis(4'-cyanobiphenyl-4-oxihexyloxy)-4,4'-diaminobiphenyl (6CBO)) [65]. Using optical second harmonic generation (SHG) and surface-enhanced Raman scattering (SERS), we found that rubbing indeed aligns the main chains along the rubbing direction, but it also causes the side chains to tilt away from the surface [65].

In this chapter, we show detailed SHG measurements and analysis of the results from a rubbed 6FDA-6CBO surface and an LC monolayer (4'-*n*-pentyl-4 cyanobiphenyl,

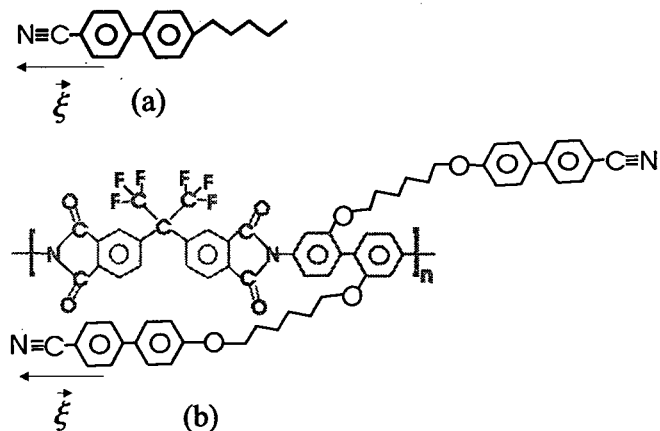


Figure 4.1: Chemical structures of (a) 5CB and (b) 6FDA-6CBO

5CB) adsorbed on it. SHG is a highly surface-specific technique [41]. With results from different input/output polarization combinations, it provides information on the surface molecular orientation. We have found that together with the main chains, the side chains are also aligned more or less along the rubbing direction, but they are bent with the free terminals pointing towards the surface. The 5CB molecules adsorbed on the surface appear to align anti-parallel to the side chains and therefore are oriented with a backward tilt with the CN terminal pointing out. This backward tilt of the surface LC molecular layer is responsible for the negative pretilt observed in the LC film sandwiched between substrates with a rubbed 6FDA-6CBO surface.

## 4.2 Theoretical background

The theory for surface SHG studies of LCs has been described in detail in the previous chapters. The SHG intensity is given in Eq. 3.1 and we can determine  $\chi_{ijk}^{(2)}$  from SHG measurements for various polarization combinations and sample orientations as described previously.

As shown in Fig. 4.1, the side chains of 6FDA-6CBO are cyanobiphenyl molecules (6OCB), each of which connects to the main chain (6FDA) through an oxygen (O) atom. Like nCB, they have a strong nonlinearity and dominate the SHG from 6FDA-6CBO [65]. In the same notation as in chapters 2 and 3, the surface nonlinear susceptibility can be expressed as

$$(\chi_{\text{CBO}}^{(2)})_{ijk} = N_S(\alpha_{\text{CBO}}^{(2)})_{\xi\xi\xi} \int (\hat{i} \cdot \hat{\xi})(\hat{j} \cdot \hat{\xi})(\hat{k} \cdot \hat{\xi})g(\theta, \phi)d\Omega, \quad (4.1)$$

with  $\alpha_{\text{CBO},\xi\xi\xi}^{(2)}$  the dominant component in a rod-like molecule. For a rubbed surface with  $C_{1v}$  symmetry, nonvanishing independent  $\chi^{(2)}$  elements and the orientational distribution,  $g(\theta, \phi)$ , of the side chains can be described by Eqs. 2.11 and 2.12, respectively. Again, the five parameters in Eq. 2.12 will provide an approximate orientational distribution for the side chains.

For a 5CB monolayer on rubbed 6FDA-6CBO, SHG measurements yield the effective nonlinear susceptibility

$$\begin{aligned} |\chi_{\text{T,EFF}}^S(\Phi)| &= |\chi_{\text{CBO,EFF}}^S(\Phi) + \chi_{\text{5CB,EFF}}^S(\Phi)| \\ &= |\chi_{\text{CBO,EFF}}^S(\Phi)| + |\chi_{\text{5CB,EFF}}^S(\Phi)|e^{i\varphi}. \end{aligned} \quad (4.2)$$

Knowing  $|\chi_{\text{CBO,EFF}}^S(\Phi)|$  from the measurement of the bare 6FDA-6CBO surface and measur-

ing the relative phase  $\varphi$ , we can deduce  $|\chi_{5\text{CB,EFF}}^S(\Phi)|$  from Eq. (4.2). As discussed earlier, we can then find  $(\chi_{5\text{CB}}^{(2)})_{ijk}$ , from which, knowing that 5CB is also a rod-like molecule, we can use Eqs. (4.1) and (2.12) to find an approximate orientational distribution function for the 5CB monolayer.

### 4.3 Experiment

The samples of 6FDA-6CBO polymer films on fused quartz substrates were prepared by spin-coating. The polymer was first dissolved in cyclopentanone (10 wt.%) and filtered with a Teflon filter (0.45  $\mu\text{m}$ ). It was then spin-coated (2000 rpm, 30 sec) on the quartz plates, baked at 120°C for 20 hours, and rubbed once with a velvet cloth. The rubbing conditions were as follows: the rotational speed of a rubbing roller is 340 rpm, the translational speed of a substrate stage 1.7 mm/sec, and the pile impression 1 mm. Further rubbing decreased SHG from the sample. There was no further treatment of the samples after rubbing. The film thickness was about 640 nm. Its refractive indices, as measured by a commercial Sopra ellipsometer, were 1.67 at 532 nm and  $1.85+0.32i$  at 266 nm. The optical density (OD) of the film at 266 nm was 4.2. With our input laser beam at 532 nm from the air side, this makes SHG in reflection from the polymer-quartz interface negligible.

The SHG experimental arrangement has been described in detail in chapter 2. The sample was mounted on a 360° rotational stage and the dependence of SHG on the azimuthal angle  $\Phi$  was measured by varying  $\Phi$  from 0° to 350° in 10° increments. The resultant  $|\chi_{\text{EFF}}^S(\Phi)|$  then allowed us to deduce  $\chi_{ijk}^{(2)}$  accurately. As the surface structure of 6FDA-6CBO could change with time after rubbing, we generally would wait for  $\sim 6$  hours

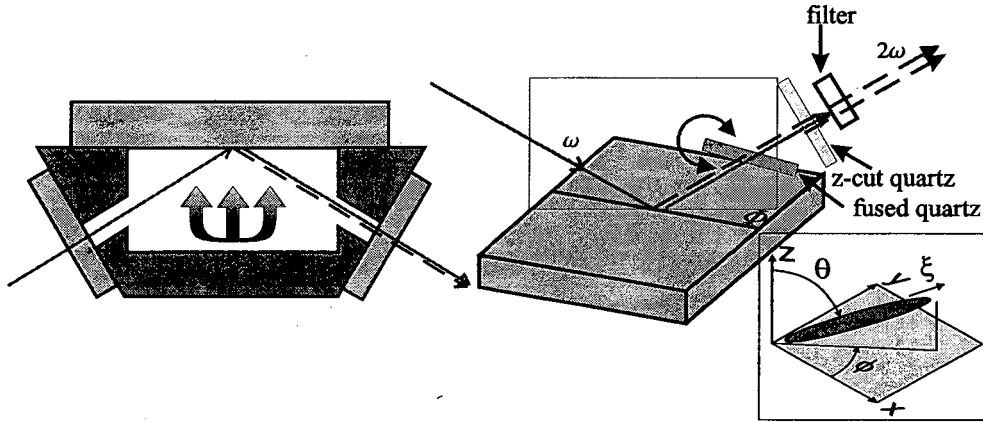


Figure 4.2: Schematics showing the experimental arrangements for (a) 5CB deposition on a substrate and (b) SHG phase measurement. Fundamental and second harmonic beams are depicted by solid and dashed lines, respectively. Inset: Coordinate systems defining the orientation of a rod-like molecule.

before we started the SHG measurements. We also chose a few different spots on the surface to avoid possible laser damage. We collected SHG data for four different input/output polarization combinations:  $S_{in}S_{out}$ ,  $S_{in}P_{out}$ ,  $P_{in}S_{out}$ , and  $P_{in}P_{out}$ .

To study a 5CB monolayer on rubbed 6FDA-6CBO, the sample was prepared by thermal evaporation using an oven temperature of  $60^{\circ}\text{C}$  (Fig. 4.2 (a)). SHG was used to monitor the deposition of 5CB on the substrate in situ. Formation of a monolayer is indicated by the leveling of the SHG signal (Fig. 4.6 (b)) because beyond the monolayer, 5CB molecules on the surface form quadrupolar pairs and contribute little to SHG [59]. The sample was then mounted on a rotational stage and SHG versus  $\Phi$  was measured.

For SHG phase measurements, we introduced a fused quartz plate of  $\frac{1}{8}''$  thickness as a phase modulator and a thin ( $50\ \mu\text{m}$ ) z-cut crystalline quartz plate (Q1) as a reference

SH generator in the reflected beam path, as shown in Fig. 4.2 (b). A similar scheme had been used previously [66]. The rotation of the fused quartz plate changes the optical path length and modulates the relative phase between the fundamental field and the reflected second harmonic field from the sample. The phase modulation causes the interference of SH fields from the sample and the reference quartz crystal (Q1) to vary and produces an interference pattern. By comparing the interference pattern with one obtained by replacing the sample with another crystalline quartz reference (Q2), the phase of  $\chi^{(2)}$  of the sample with respect to that of the quartz reference (Q2) can be deduced.

#### 4.4 Results and analysis

Shown in Fig. 4.3 are the results of SHG measurements for the four polarization combinations on rubbed 6FDA-6CBO:  $|\chi_{\text{CBO,EFF}}^S(\Phi)|^2$  versus  $\Phi$ . As discussed in Sec. 4.2, fitting the data (solid lines in Fig. 4.3) allows the determination of the six independent nonvanishing  $(\chi_{\text{CBO}}^{(2)})_{ijk}$  elements. We obtain

$$\begin{aligned} & \chi_{xxx}^{(2)} : \chi_{xyy}^{(2)} : \chi_{xzz}^{(2)} : \chi_{zxx}^{(2)} : \chi_{zyy}^{(2)} : \chi_{zzz}^{(2)} \\ = & \quad 1 : 0.23 : 0.036 : -0.076 : -0.020 : -0.020 \end{aligned}$$

with errors of  $\pm 5\%$ ,  $\pm 20\%$ ,  $\pm 10\%$ ,  $\pm 25\%$ , and  $\pm 25\%$  for the five ratios, respectively. As we mentioned earlier,  $(\chi_{\text{CBO}}^{(2)})_{ijk}$  originates mainly from the 6CBO side chains. However, it was found in a similar polyimide (6FDA-PFMB, which has the same backbone but no side chains [65]) that the field discontinuity at the surface (along  $\hat{z}$ ) contributes a value of 0.012 to  $\chi_{zzz}^{(2)}$ . This is significant compared to the above value of  $-0.020$  for  $(\chi_{\text{CBO}}^{(2)})_{zzz}$  and must be subtracted from the latter if we are only interested in the contribution of the

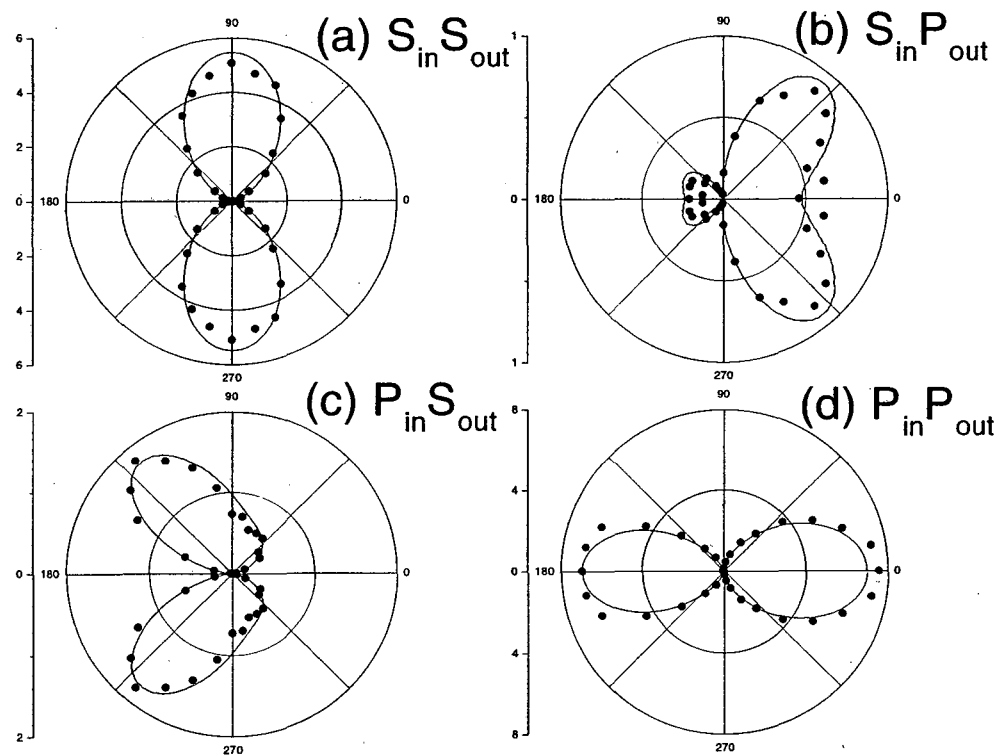


Figure 4.3: Polar plots of  $|\chi_{\text{CBO, EFF}}^S(\Phi)|^2$  (arbitrary units) versus  $\Phi$  for (a)  $S_{\text{in}}S_{\text{out}}$ , (b)  $S_{\text{in}}P_{\text{out}}$ , (c)  $P_{\text{in}}S_{\text{out}}$ , and (d)  $P_{\text{in}}P_{\text{out}}$  polarization combinations. Circles are experimental data and lines are fits.

side chains to  $(\chi_{\text{CBO}}^{(2)})_{zzz}$  for the deduction of the distribution function  $g(\theta, \phi)$  for the side chains. Contributions of the field discontinuity to the other  $(\chi_{\text{CBO}}^{(2)})_{ijk}$  elements are much weaker and can be neglected. We can then use the values of  $(\chi_{\text{CBO}}^{(2)})_{ijk}$  to determine  $g(\theta, \phi)$  following Eqs. (4.1) and (2.12). The deduced parameters for  $g(\theta, \phi)$  are listed in Table 4.1. It is interesting to note that the parameter  $d_1$  is negative. This implies that the 6CBO side chains are aligned opposite to the rubbing direction. From  $\int g(\theta, \phi) \sin \theta \, d\theta$ , we can obtain the azimuthal distribution of the side chains, as depicted in Fig. 4.8.

The SHG intensity measurements cannot distinguish between the two possible molecular orientations of the side chains in Figs. 4.4 (a) and (b). To resolve the ambiguity, we need a phase measurement. We consider here the phase of  $\chi_{xxx}^{(2)}$ . The side chains with opposite orientations illustrated in Figs. 4.4 (a) and (b) should have a  $180^\circ$  phase difference in  $\chi_{xxx}^{(2)}$  (as can be seen explicitly in Eq. (4.1) with  $\hat{\xi}$  replaced by  $-\hat{\xi}$ ). We can compare the measured phase of  $\chi_{xxx}^{(2)}$  for the 6CBO side chains with that for a 5CB monolayer adsorbed on a polyimide without side chains (P6) [58, 62]. The latter is known to have 5CB molecules oriented with the CN terminal facing the surface (Fig. 4.4 (c)). As seen from the measured interference patterns for the two cases in Figs. 4.4 (d) and (e), the phase of  $\chi_{xxx}^{(2)}$  of 5CB on P6 is opposite to that of 6CBO. The correct orientation of the 6CBO side chains therefore must be the one shown in Fig. 4.4 (a). We also found that the phases of  $\chi_{zxx}^{(2)}$  for the 6CBO side chains and the 5CB monolayer are the same, consistent with the pictures in Figs. 4.4 (a) and (c). As we shall see later, this orientation of the 6CBO side chains is responsible for the observed negative pretilt of the bulk LC alignment.

The results of SHG measurements of  $|\chi_{\text{T,EFF}}^S(\Phi)|^2$  versus  $\Phi$  on a 5CB monolayer

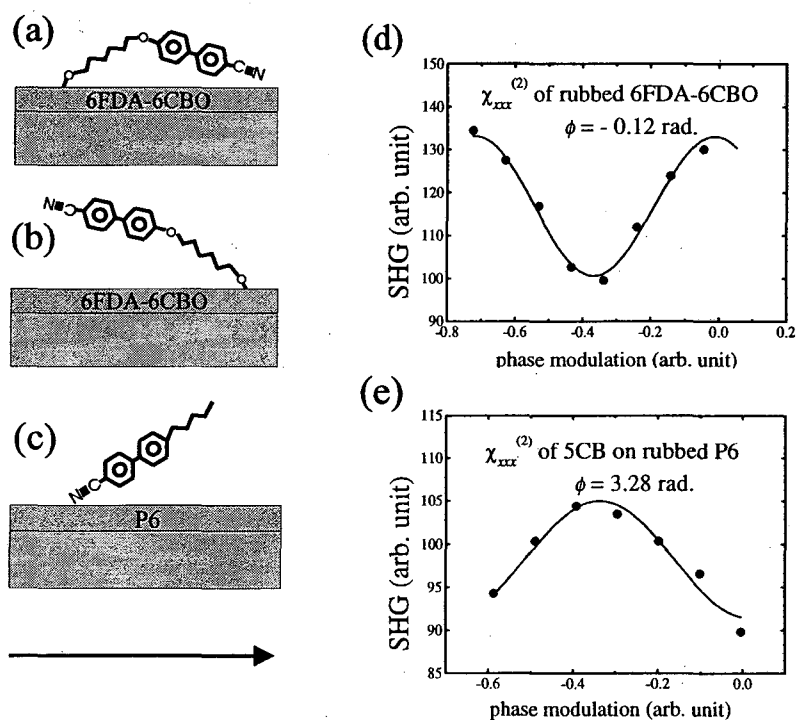


Figure 4.4: Schematics describing the two possible orientations of the 6CBO side chains in (a) and (b) and the orientation of 5CB molecules adsorbed on a polyimide (P6) surface in (c). The experimental data and the line fits in (d) and (e) describe the results of SHG phase measurements of  $(\chi_{\text{CBO}}^{(2)})_{xxx}$  and  $(\chi_{5\text{CB}}^{(2)})_{xxx}$ , respectively. The arrow denotes the rubbing direction.

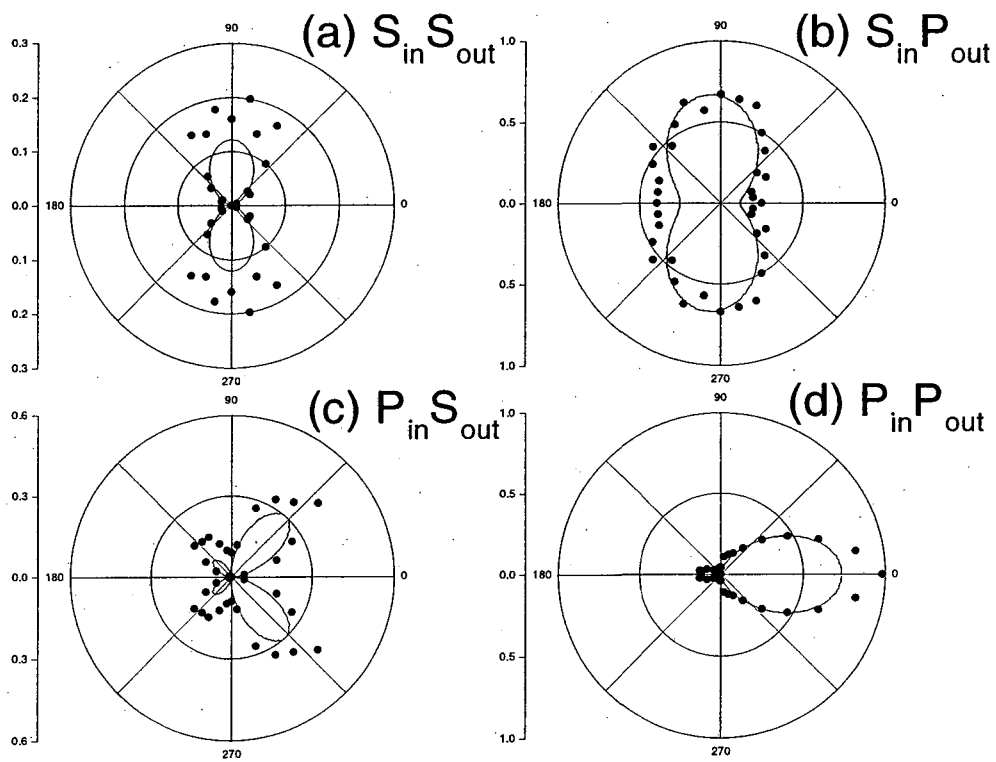


Figure 4.5: Polar plots of  $|\chi_{T, \text{EFF}}^S(\Phi)|^2$  (arbitrary units) versus  $\Phi$  for (a)  $S_{\text{in}} S_{\text{out}}$ , (b)  $S_{\text{in}} P_{\text{out}}$ , (c)  $P_{\text{in}} S_{\text{out}}$ , and (d)  $P_{\text{in}} P_{\text{out}}$  polarization combinations. Circles are experimental data and lines are fits.

Table 4.1: Parameters in orientational distribution function  $g(\theta, \phi)$  for 6FDA-6CBO and 5CB monolayer

	6FDA-6CBO	5CB
$\theta_0$	$86.5 \pm 1.$	$81.4 \pm 1$
$\sigma$	$9.5 \pm 1.$	$10.5 \pm 0.5$
$d_1$	$-1.4 \pm 0.4$	$-0.81 \pm 0.1$
$d_2$	$1.2 \pm 0.2$	$0.79 \pm 0.05$
$d_3$	$-0.38 \pm 0.15$	$-0.20 \pm 0.05$

on rubbed 6FDA-6CBO for four polarization combinations are given in Fig. 4.5. In order to determine  $\chi_{5\text{CB,EFF}}^S(\Phi)$ , we used Eq. (4.2) in which  $|\chi_{\text{CBO,EFF}}^S(\Phi)|$  was already obtained and  $\varphi$  measured by SHG phase measurement to be  $0.26 \pm 0.3$  rad. Within the error of our measurement,  $\varphi$  was found to be independent of input/output polarization combinations or sample orientations, as expected from rod-like molecules. Thus, fitting of the measured  $|\chi_{\text{T,EFF}}^S(\Phi)|^2$  with  $(\chi_{5\text{CB}}^{(2)})_{ijk}$  as adjustable parameters allows us to determine the six nonvanishing  $(\chi_{5\text{CB}}^{(2)})_{ijk}$ . After normalization against  $(\chi_{\text{CBO}}^{(2)})_{xxx}$ , they are

$$\begin{aligned} & \chi_{xxx}^{(2)} : \chi_{xyy}^{(2)} : \chi_{xzz}^{(2)} : \chi_{zxx}^{(2)} : \chi_{zyy}^{(2)} : \chi_{zzz}^{(2)} \\ = & -0.81 : -0.191 : -0.028 : 0.23 : 0.101 : 0.041 \end{aligned}$$

with errors of  $\pm 4\%$ ,  $\pm 10\%$ ,  $\pm 20\%$ ,  $\pm 5\%$ ,  $\pm 10\%$ , and  $\pm 12\%$ , respectively. From these values of  $(\chi_{5\text{CB}}^{(2)})_{ijk}$ , we can again use Eqs. (4.1) and (2.12) to find  $g(\theta, \phi)$  for the 5CB monolayer. The deduced parameters for  $g(\theta, \phi)$  of 5CB are also listed in Table 4.1. We note that  $(\chi_{5\text{CB}}^{(2)})_{xxx}$  and  $(\chi_{\text{CBO}}^{(2)})_{xxx}$  have opposite signs, indicating that the 5CB molecules and the CBO side chains have anti-parallel orientations along the rubbing direction (Fig. 4.6 (a)). This is well confirmed by the in situ SHG measurement monitoring 5CB deposition on 6FDA-6CBO described in Fig. 4.6 (b). The data showing the decay of  $|\chi_{\text{T,EFF}}^S(\Phi)|^2$  with 5CB deposition is a clear indication that the adsorbed 5CB molecules and the 6CBO

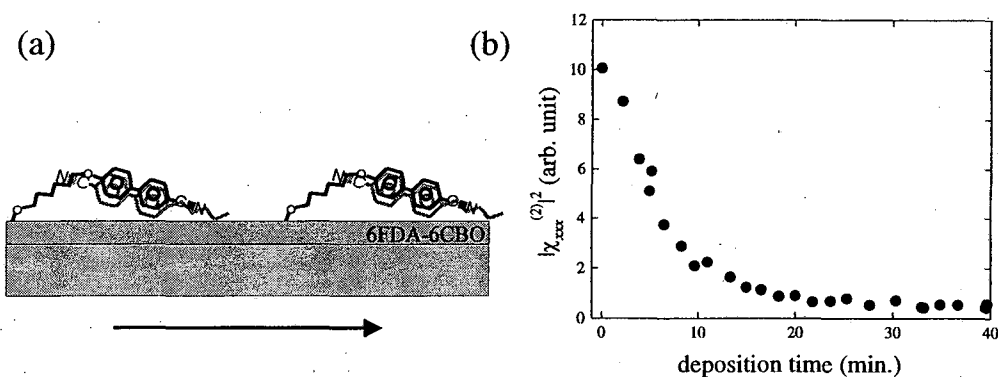


Figure 4.6: (a) Schematic showing the orientations of adsorbed 5CB molecules and 6CBO side chains on a rubbed 6FDA-6CBO surface. The arrow denotes the rubbing direction. (b)  $|\chi_{T,EFF}^{(2)}|^2$  as a function of 5CB evaporation time obtained by in situ SHG monitoring of 5CB deposition on 6FDA-6CBO.

side chains have opposite orientations. As shown in Fig. 4.8, the azimuthal distribution of the 5CB monolayer obtained from  $\int g(\theta, \phi) \sin\theta d\theta$  is well correlated with that of the side chains. A 5CB film sandwiched between two substrates coated with rubbed 6FDA-6CBO (Fig. 4.7) appeared to be well aligned homogeneously along the rubbing direction. From an ellipsometry measurement (Ref. [67]), the bulk pretilt angle was found to be

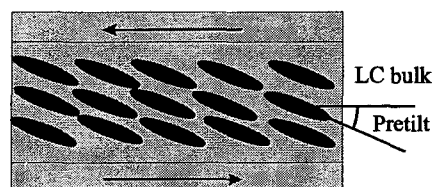


Figure 4.7: Schematic describing the negative pretilt angle of a 5CB film sandwiched between two rubbed 6FDA-6CBO surfaces. The arrows denote the rubbing directions on the two substrates.

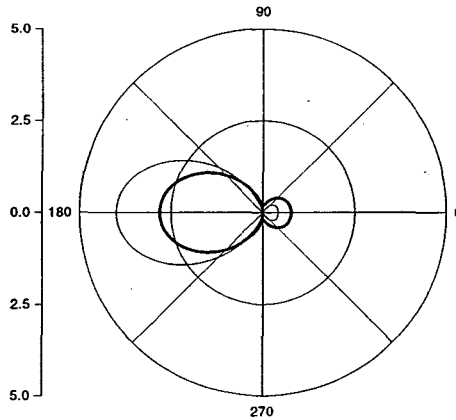


Figure 4.8: Azimuthal orientational distributions of side chains (thin line) and 5CB molecules in an adsorbed monolayer (thick line) on a rubbed 6FDA-6CBO surface.

$\alpha_b = -8.7^\circ$ . This negative pretilt angle is induced through LC molecular correlation by the orientation of molecules in the surface LC monolayer, which is anti-parallel to the rubbing direction (Fig. 4.7). Assuming boundary surfaces fully covered with 5CB molecules with the orientational distribution specified in Table 4.1, we can use the Landau-de Gennes theory to calculate the pretilt angle [58]. We found  $\alpha_b = -4.4^\circ$ . The discrepancy between theory and experiment is presumably because, in reality, the boundary surfaces are composed of a mixture of oriented 5CB molecules and 6CBO side chains.

## 4.5 Discussion

SHG is highly surface-specific and sensitive, but is not necessarily helpful in the determination of surface molecular orientation unless the molecule is highly symmetric [43]. Fortunately, this is the case for both 6CBO side chains and 5CB molecules. The second-order

nonlinear polarizabilities for both 6CBO and 5CB are dominated by the cyanobiphenyl chromophores, which appear to have no strongly preferred orientation about their long molecular axes. Thus they can be treated as rod-like molecules, and as shown in the previous section, SHG can be used to determine approximate orientational distributions of the chromophores.

It is known that rubbing can align the main chains of a polymer at the surface [26, 28, 34, 68]. This has been found to be true for a number of polyimides including 6FDA-6CBO. What we have observed here, in addition, is that the side chains are also aligned by rubbing, which is not always the case [29]. The reason is that the polar 6CBO side chains here are connected to the main chains through a  $(\text{CH}_2)_6$  section that can be bent by creation of trans-cis defects. The chromophores are expected to orient along the rubbing direction. Since the terminal CN of 6CBO has an attractive interaction with the polyimide main chain, the chromophores would have a polar orientation with a tilt in the direction anti-parallel to rubbing (Fig. 4.4 (a)), as we have observed.

On polyimides without side chains, 5CB molecules are known to adsorb with the CN terminal anchored to the main chain. With the 6CBO side chains, however, this is no longer the case. We now have the polar orientation of adsorbed 5CB molecules inverted, *i. e.*, the CN terminal is pointing away from the surface. Apparently, the interaction between 5CB and 6CBO chromophores dominates and favors the anti-parallel pair interaction geometry normally observed in bulk LC. Rubbing aligns the 6CBO side chains, which in turn, align the adsorbed 5CB molecules. The azimuthal orientational distributions of 6CBO and 5CB chromophores are therefore correlated (Fig. 4.8).

The pretilt angle of a homogeneously aligned LC film is determined by the molecular orientations in the boundary layers. In our case, the observed negative pretilt is obviously induced by the orientations of 6CBO and 5CB at the surface, which are opposite to the rubbing direction. As to a quantitative estimate of the pretilt, unfortunately, we do not yet know how to describe properly the orientational boundary conditions for LCs presented by a mixed monolayer of 6CBO and 5CB.

The goal of many who works on LCDs is to have a large, controllable pretilt angle. Our work here indicates that this may be possible with side-chain polyimides if the side chains have an appropriate structure. For a large pretilt, we need side chains that can be aligned by rubbing and have a large tilt away from the surface. They must also interact with LC molecules sufficiently strongly so that they can effectively align the latter. We can imagine, for example, a modification of 6FDA-6CBO. Instead of attaching 6CBO directly to the 6FDA main chain, let it be attached through a stiff molecular stem projecting vertically out from the main chain and from the surface. This way, 6CBO side chains retain all their characteristic features for LC alignment, but the additional spacing between 6CBO and the main chain, effected by the molecular stem, would allow 6CBO to have a larger tilt at the surface. Varying the length of the stem could change the tilt angle of 6CBO and hence the pretilt of the LC film.

## 4.6 Conclusions

Surface SHG allowed the determination of approximate orientational distributions of 6CBO side chains on a rubbed 6FDA-6CBO surface and 5CB molecules adsorbed on the surface.

There is a strong correlation between the two. Both are highly anisotropic, preferentially aligned along the rubbing direction. The molecular tilts away from the surface, however, are in the anti-rubbing direction. This leads to the negative pretilt we observed in the homogeneously aligned LC film sandwiched between substrates coated with rubbed 6FDA-6CBO. The orientations of 6CBO and 5CB at the surface were found to be anti-parallel, as one would expect from the pair interaction geometry of such molecules. Our results here provide us with some insight into possible exploitation of side-chain polymers to control the pretilt angle of an LC display cell.

## Chapter 5

# Orientations of phenyl sidegroups and liquid crystal molecules on a rubbed polystyrene surface

### 5.1 Introduction

Mechanical rubbing of polymer surfaces is a technique commonly used to align liquid crystal (LC) films for LC devices [44]. Recent studies have found that rubbing aligns the surface polymer chains [26, 30, 34], which in turn align the LC molecules adsorbed on the surface and then molecules throughout the bulk film [58]. Infrared-visible sum-frequency vibrational spectroscopy (SFVS) and second-harmonic generation (SHG) are effective probes for such studies. Being surface-specific, they allow quantitative determination of molecular orientation and alignment at a polymer surface. Applications of the techniques to rubbed

surfaces of polyvinyl alcohol (PVA) and polyimide (PI) have shown that the surface polymer chains are well aligned along the rubbing direction, and so are the LC molecules adsorbed on them [26, 30, 32]. Rubbing of a polystyrene ( $-\text{[CH}_2\text{-CH(C}_6\text{H}_5)\text{]}-\text{n}$ : PS) surface, however, is known to induce an LC film alignment perpendicular to the rubbing direction [43, 47]. One would then expect that if rubbing aligns the polymer chains along the rubbing direction, the phenyl sidegroups protruding out of the surface must have an orientation perpendicular to the rubbing. The latter must interact more effectively with the adsorbed LC molecules than the main chains in inducing the LC alignment. To confirm this picture, we have conducted SFVS on a rubbed PS and SHG on LC adsorbed on a rubbed PS. In this chapter, we show our findings.

## 5.2 Experiment

The experimental setup and the theoretical background for SFVS and SHG have been described in chapter 2. The samples used were isotactic PS films with a layer thickness of  $\sim 400$  nm prepared by spin-coating. To obtain an uniform layer, the PS solution in toluene (Scientific Polymer Products, Inc.) was filtered by membrane filters. It was then dropped on a substrate to be spin-coated at 3500 rpm for 60 seconds. The samples were then baked at  $170^\circ\text{C}$  for 60 minutes. Rubbing of a PS surface was carried out by a rubbing machine with a velvet cloth.

### 5.3 Results, analysis, and discussion

Figure 5.1 presents the SFVS spectra in the CH stretch region of a rubbed PS/air interface taken at three different angles ( $\Phi = 0^\circ$ ,  $90^\circ$ , and  $180^\circ$ ) between the incidence plane and the rubbing direction with three input/output polarization combinations: SSP (denoting S-polarized SF output, S-polarized visible input, and P-polarized infrared input, respectively), PPP, and SPS. The spectra exhibit five aromatic CH vibrational stretches associated with the phenyl sidegroups. They appear at 3024, 3036, 3057, 3069, and 3084  $\text{cm}^{-1}$ , which can be assigned to the  $\nu_{20b}$ ,  $\nu_{7a}$ ,  $\nu_{7b}$ ,  $\nu_2$ , and  $\nu_{20a}$  vibrational modes, respectively [69].

SFVS on PS films has recently been reported by several groups [70, 71]. In all investigations, it was concluded that the observed SF signal is dominated by the contribution from the PS/air interface. Therefore in our case, we can consider SF signals in Fig. 5.1 as coming mainly from the phenyl sidegroups projecting out of the PS surface.

We now focus on the symmetric stretch  $\nu_2$  at 3069  $\text{cm}^{-1}$  of the phenyl group as it is most prominent in the spectra. This mode can be strongly excited by an IR field along  $\hat{\zeta}$  in the molecular coordinates described in Fig. 5.2 and by Raman excitation with a symmetric polarizability tensor component in the  $\xi$ - $\zeta$  plane. Thus, the nonlinear polarizability for SFVS in resonance with this mode is dominated by components  $\alpha_{\zeta\zeta\zeta}^{(2)}$  and  $\alpha_{\xi\xi\zeta}^{(2)}$ . From the SF spectra, we can readily obtain a qualitative picture of the rubbing-induced alignment of the phenyl sidegroups. First, the SSP spectra at  $\Phi = 0^\circ$  and  $\Phi = 180^\circ$  are significantly stronger than the one at  $\Phi = 90^\circ$ , indicating that the phenyl sidegroups are more or less along the direction perpendicular to the rubbing direction. Second, the hardly detectable forward-backward asymmetry in the spectra suggests that the phenyl groups do not have

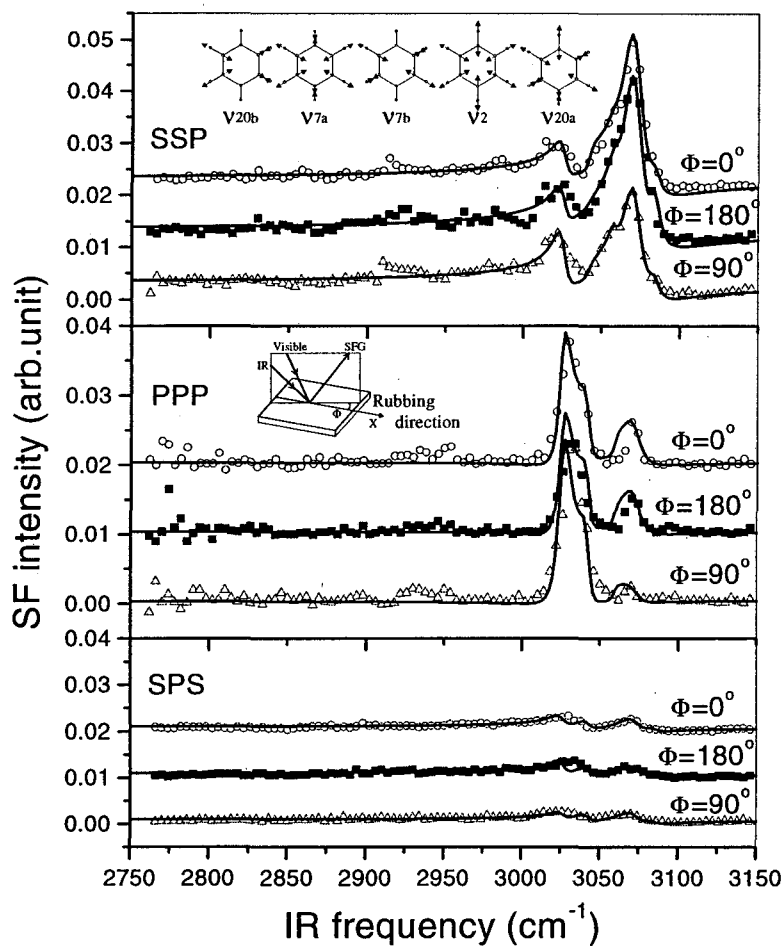


Figure 5.1: SFVS spectra with (a) SSP, (b) PPP and (c) SPS polarization combinations for a rubbed isotactic PS film. The inset of the top graph shows the normal mode vibrations of the aromatic CH stretch. The angle  $\Phi$  between the incidence plane and the rubbing direction describes the azimuthal orientation of the sample. The spectra are normalized by the SF signal from a z-cut quartz.

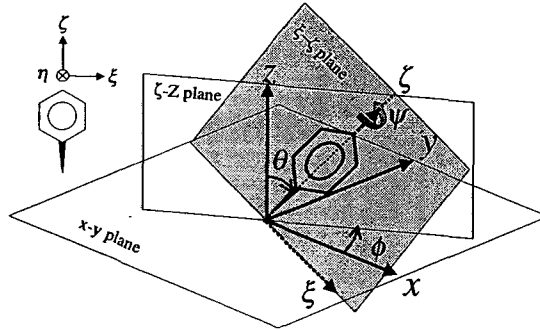


Figure 5.2: Geometric relations between the molecular coordinates and the laboratory coordinates. The rubbing direction is defined along  $x$  axis.

an appreciable tilt toward the rubbing direction, or the polymer backbones lie nearly flat on the surface. The observed azimuthal anisotropy is relatively small compared to the cases of rubbed PVA and PI. This is partly because we rubbed PS only gently to avoid possible removal of the PS film from the substrate. The degree of anisotropy in the spectra is a measure of how broad a distribution the chain orientation has around its mean.

More quantitatively, we can deduce the orientational distribution function of the phenyl sidegroup using the the same analysis described in Ref. [26]. We present only a brief sketch of the procedure below. The nonlinear susceptibility  $\chi^{(2)}$  responsible for SFVS can be written as

$$\begin{aligned} \vec{\chi}^{(2)} &= \vec{\chi}_{\text{NR}}^{(2)} + \sum_q \frac{\vec{A}_q}{\omega_2 - \omega_q + i\Gamma_q}, \quad \text{with} \quad (5.1) \\ \vec{A}_q &= N_s \int \vec{a}_q(\Omega) f(\Omega) d\Omega. \end{aligned}$$

Here  $\vec{\chi}_{\text{NR}}^{(2)}$  denotes the nonresonant contribution;  $\vec{a}_q$ ,  $\omega_q$ , and  $\Gamma_q$  are the strength, resonant frequency, and damping constant, respectively, of the  $q^{\text{th}}$  resonant vibrational mode;  $\Omega$

Table 5.1: Parameters used in the calculation of  $(A_q)_{ijk}$  and measured and calculated nonvanishing tensor elements  $(A_q)_{ijk}$  for the  $\nu_2$  mode of the phenyl stretch.  $\epsilon'_{\text{SF}} \approx \epsilon'_{\text{vis}} \approx 1.6$  and  $\epsilon'_{\text{IR}} \approx 1.2$ .

	$\omega_s$	$\omega_1$	$\omega_2$
wavelength $\lambda/\mu\text{m}$	0.457	0.532	3.26
refractive index $n(\text{polystyrene})$	1.61	1.59	1.56
$n(\text{fused quartz})$	1.47	1.46	1.41
beam angle $\beta/\text{deg.}$	46.5	45.0	57.0
fresnel factor $L_{xx}$	0.861	0.906	0.982
fresnel factor $L_{yy}$	0.598	0.695	0.554
fresnel factor $L_{zz}$	$1.139/\epsilon'_{\text{SF}}$	$1.094/\epsilon'_{\text{vis}}$	$1.019/\epsilon'_{\text{IR}}$

	measured	calculated
$A_{xxz}$	$3.1 \pm 0.2$	3.1
$A_{yyz}$	$3.9 \pm 0.2$	3.9
$A_{zzz}$	$3.3 \pm 0.3$	3.2
$A_{xzx} = A_{zxx}$	$1.2 \pm 0.2$	1.2
$A_{yzy} = A_{zyy}$	$1.9 \pm 0.3$	2.0

represents a set of orientational angles  $(\theta, \phi, \psi)$  for a phenyl ring;  $N_s$  is the surface density of the phenyl groups; and  $f(\Omega)$  is the orientational distribution function of the phenyl groups. The  $C_{2v}$  symmetry of a rubbed surface without forward-backward asymmetry allows only five independent nonvanishing elements of the third-rank tensor  $A_q$  for each vibrational mode:  $(A_q)_{xxz}$ ,  $(A_q)_{yyz}$ ,  $(A_q)_{zzz}$ ,  $(A_q)_{xzx}=(A_q)_{zxx}$ ,  $(A_q)_{yzy}=(A_q)_{zyy}$  [26]. They can be determined, together with the other parameters, from fitting of the SF spectra obtained with different sample orientations ( $\Phi$ ) and input/output polarization combinations. For the  $\nu_2$  mode of PS, the deduced values of  $(A_q)_{ijk}$  and the other parameters are listed in Table 5.1. To find  $f(\Omega)$ , we know that, for the  $\nu_2$  mode, the dominant tensorial elements of  $\vec{a}_q$  in the molecular coordinates are  $(a_q)_{\xi\xi\xi}$  and  $(a_q)_{\zeta\zeta\zeta}$ , which can be transformed into the laboratory coordinates  $(i, j, k)$  as functions of  $\Omega = (\theta, \phi, \psi)$ . Then knowing the values

of  $(A_q)_{ijk}$  and assuming that  $f(\Omega)$  can be approximated by a Gaussian form

$$f(\Omega) = C \exp\left(-\frac{(\theta - \theta_0)^2}{2\sigma_\theta^2} - \frac{(\phi - \phi_0)^2}{2\sigma_\phi^2} - \frac{(\psi - \psi_0)^2}{2\sigma_\psi^2}\right), \quad (5.2)$$

we can determine  $(a)_{\zeta\zeta\zeta}/(a)_{\xi\xi\xi}$  and all the parameters in Eq. 5.2. We have found  $(a)_{\zeta\zeta\zeta}/(a)_{\xi\xi\xi} = 1.68 \pm 0.15$ ,  $\phi_0 = 90^\circ$ ,  $\sigma_\phi = 49^\circ \pm 5^\circ$ ,  $\psi_0 = 90^\circ$ ,  $\sigma_\psi = 68^\circ \pm 9^\circ$ , and  $\theta_0$  in the range from  $72^\circ \pm 6^\circ$  to  $83^\circ \pm 7^\circ$  with  $\sigma_\theta$  varying from  $\sim 3^\circ$  at  $\theta_0 = 72^\circ$  to  $\sim 17^\circ$  at  $\theta_0 = 83^\circ$ . To show the consistency of the result, we used the deduced  $f(\Omega)$  to reevaluate  $(A_q)_{ijk}$ . The calculated values of  $(A_q)_{ijk}$ , also listed in Table 5.1, are indeed close to those deduced from the measurements.

We also used SHG to study the orientation of 4'-*n*-pentyl-4-cyanobiphenyl (5CB) adsorbed on PS. The LC molecules were deposited on PS by thermal evaporation. During the evaporation, in situ measurement showed that SHG increased monotonously and then leveled off [59]. The saturated signal from the 5CB layer was rather weak, less than one tenth of that from a 5CB monolayer on PI (P6). The ratio of  $\chi^{(2)}$  of PS to  $\chi^{(2)}$  of 5CB on PS was around 1 : 1.4. This indicates that polar adsorption of 5CB on the nonpolar PS surface is probably poor, leading to only a partial coverage of the surface by polar-oriented 5CB molecules. That the surface was actually partly covered by 5CB molecules with their CN terminals toward the surface was found from an SHG phase measurement [30]. As shown in Fig. 5.3 (a), interference of the SHG signals from 5CB on rubbed PS and on *n*-hexyl pyromellitic polyimide (P6) with that from a quartz plate yielded the phase  $\varphi$  of  $\chi^{(2)}$  for the two cases. SHG from 5CB on P6 is dominated by a contribution from 5CB molecules that adsorb with the CN terminal facing P6 [43, 72]. Therefore  $\chi_{5CB}^{(2)} \sim \chi_{5CB/P6}^{(2)}$ . The vector diagram of  $\chi^{(2)}$  in Fig. 5.3 (b) shows that the polar-oriented 5CB molecules on PS must

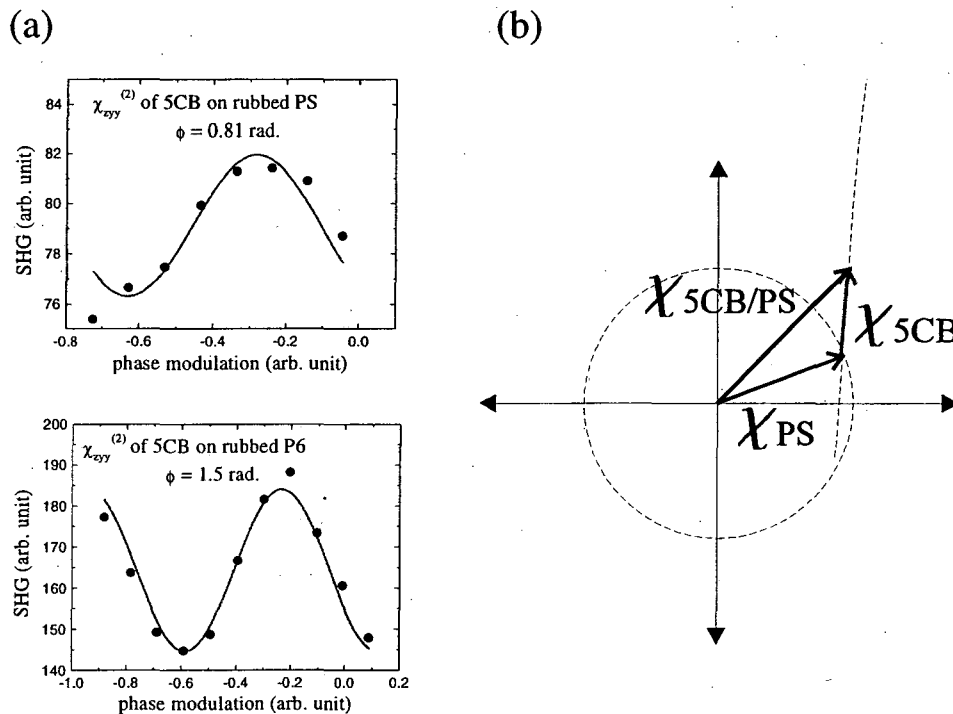


Figure 5.3: (a) Experimental data and curve fits for SHG phase measurements of 5CB monolayers on rubbed PS and P6, respectively. (b) Schematic phase relationship of  $\chi^{(2)}$  for a 5CB monolayer on a PS surface.  $\chi_{\text{PS}}^{(2)}$ ,  $\chi_{\text{5CB}}^{(2)}$  and  $\chi_{\text{PS/5CB}}^{(2)}$  are the susceptibilities of the PS surface, the 5CB monolayer, and the 5CB monolayer on rubbed PS, respectively.

also have their CN terminals facing PS; an opposite orientation of 5CB would change the sign of  $\chi_{\text{5CB}}^{(2)}$  and would lead to an SHG signal from 5CB/PS that decreases with increasing 5CB coverage, contrary to the observation.

It is interesting to note that we have found equal SHG signals (in reflection) from homogeneous 5CB films sandwiched between rubbed PS substrates and between rubbed PVA substrates, despite the significant difference of SHG from evaporated 5CB layers on

PS and PVA. This indicates that in the presence of the bulk 5CB film, the 5CB molecules at the PS surface are forced to assume a polar orientation with CN facing the surface as in the case of 5CB on PVA [26]. Presumably when 5CB molecules are forced to be next to the phenyl rings, they would prefer to have their biphenyl cores interact with the phenyl rings, and hence have their CN terminals toward the surface. We have also found, from a 5CB film sandwiched between rubbed PS surfaces, stronger SHG with the input polarization perpendicular to the rubbing direction than parallel to the rubbing direction, indicating that 5CB molecules in the film were aligned perpendicular to the rubbing direction. This was also verified by linear optical measurements.

## 5.4 Conclusions

We have shown that mechanical rubbing effectively aligns the surface phenyl sidegroups of PS perpendicular to the rubbing direction. The phenyl planes incline towards the surface with a rather broad distribution. The aligned phenyl sidegroups at the PS surface can interact with nearby 5CB molecules and force them to polar-orient with the CN terminals facing the surface. The orientation and alignment of the 5CB surface monolayer can then induce a homogeneous alignment of the 5CB bulk film through molecular correlation.

## Chapter 6

# Rubbing-Induced Polar Ordering of Nylon 11

### 6.1 Introduction

Nylon is among the first and most important synthetic polymers developed and used in modern life. In the last decade, odd-numbered nylons, *i.e.*, nylons with an odd number of carbon atoms in each repeating unit, have attracted much attention for their ferroelectric properties [15]. As shown in Fig. 6.1 (a), for an odd-numbered nylon such as nylon 11, a macroscopic polarization can be achieved by the parallel alignment of the dipoles associated with the amide units. Ferroelectric hysteresis has been observed in nylon 11 films prepared by cold-drawing and poling [15]. In contrast, an even-numbered nylon such as nylon 6 cannot form a macroscopic polarization (Fig. 6.1 (b)). Ferroelectric nylon films are potentially useful in many applications including audiofrequency and ultrasonic trans-

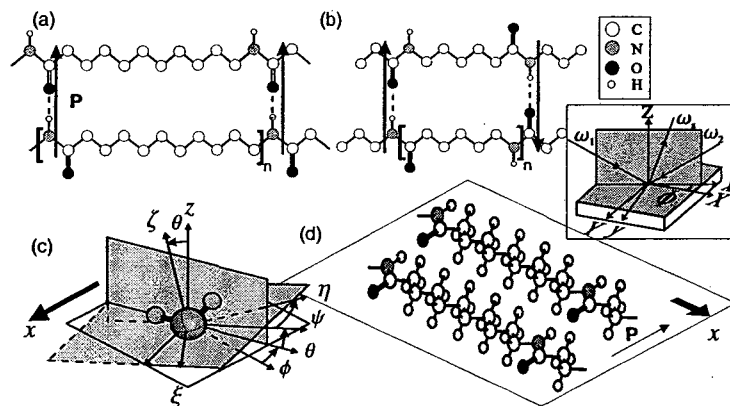


Figure 6.1: Chemical structure of (a) nylon 11 and (b) nylon 6. The arrows (**P**) are dipoles and the dotted lines hydrogen bonds. (c) The molecular orientation of CH<sub>2</sub>. (d) The molecular picture of rubbed nylon 11.  $x$  is along the rubbing direction,  $z$  along the surface normal of the polymer film,  $\zeta$  along the symmetry axis of CH<sub>2</sub> and that of NH and CO bonds, and  $\xi$  normal to the CH<sub>2</sub> plane and along the chain direction. Inset: geometry of the incidence plane with respect to the sample surface.  $\Phi$  is an angle between  $x$  and the incidence plane.

ducers, pyroelectric detectors, robotics, and biosensors [5]. Nylon films can also serve as templates for adsorbing biomolecules such as nucleic acids and proteins [73, 74]. Therefore it is important to have a good understanding of the fabrication and characterization of such polar-ordered nylon films. In this study, sum-frequency vibrational spectroscopy (SFVS) was employed to study the structural change of nylon thin films before and after mechanical rubbing. Being a second order nonlinear optical technique, SFVS is ideally suited as a probe to study polar ordering in polymer thin films. We found that for nylon 11, mechanical rubbing is capable of aligning the polymer chains and forming a large in-plane ferroelectric polarization perpendicular to the rubbing direction (Fig. 6.1 (d)). A possible mechanism will be suggested.

## 6.2 Background

The experimental setup (see also the inset in Fig. 6.1) and theoretical background for SFVS have been described in chapter 2. A pellet of nylon 11 ( $[-\text{NH-CO}-(\text{CH}_2)_{10}]_n-$ ) was baked overnight at  $100^\circ\text{C}$  to remove water. A nylon film on a fused quartz substrate was prepared by pressing it with a hydrophobic quartz substrate coated with octadecyltrichlorosilane (OTS) above the melting temperature of nylon 11 and separating it from the OTS-coated substrate by weakly shearing the OTS-coated substrate against the film after quenching in liquid nitrogen. It was then rubbed with a velvet cloth. In the experiment, sum frequency ( $\omega_s$ ) was generated from  $\omega_1$  ( $= 1.064 \mu\text{m}$ ) and  $\omega_2$  (tunable IR). The tunable IR covers the spectral ranges for the vibrational modes of CO ( $1500 \sim 1700 \text{ cm}^{-1}$ ), CH<sub>2</sub> ( $2800 \sim 3000 \text{ cm}^{-1}$ ), and NH ( $3150 \sim 3450 \text{ cm}^{-1}$ ). The SF field is proportional to the effective nonlinear susceptibility defined as  $\chi_{\text{EFF}}^{\text{S}} = (\vec{L}(\omega_s) \cdot \hat{e}(\omega_s)) \cdot \overset{\leftrightarrow}{\chi}_{\text{S,eff}}^{(2)} : (\vec{L}(\omega_1) \cdot \hat{e}(\omega_1))(\vec{L}(\omega_2) \cdot \hat{e}(\omega_2))$ , where  $\hat{e}(\omega_i)$  is the unit polarization vector at  $\omega_i$ , and  $\vec{L}(\omega_i)$  is the macroscopic local field correction tensor (Eq. 2.6):  $\overset{\leftrightarrow}{\chi}_{\text{S,eff}}^{(2)}$  in a uniform bulk film is given in Eq. 2.3 and the subscript S,eff is omitted hereafter.

## 6.3 Results and analysis

Shown in Fig. 6.2 are the SF spectra for isotropic nylon 11 (nylon 11 before rubbing) with three polarization combinations (SSP (denoting S-polarized SF output, S-polarized  $\vec{E}(\omega_1)$  input, and P-polarized  $\vec{E}(\omega_2)$  input), PPP, and SPS). No NH signal was observed, suggesting the NH groups are not polarized and presumably lie in plane. Shown in Fig. 6.3 are the SF spectra for rubbed nylon 11 for various polarization combinations and the relative

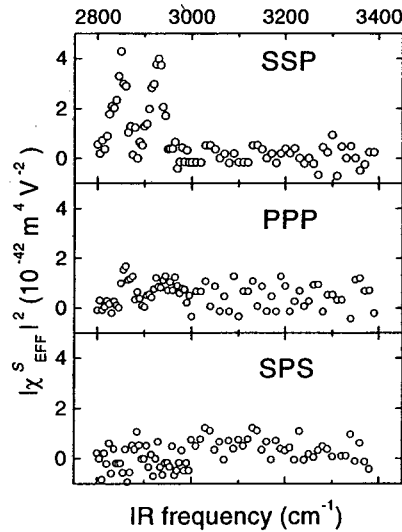


Figure 6.2: SF spectra of isotropic nylon 11.

orientations ( $\Phi$ ) between the rubbing direction and the incidence plane of the beams (see the inset of Fig. 6.1). Only the SF spectra of SSP, PPP, PPS, and SSS are presented, the others showing only small spectral peaks. More than 100-fold signal enhancement was observed after rubbing, which cannot be explained by the surface contribution. The bulk contribution to SFVS actually dominates, as will be shown later. The large difference in the signal levels for different orientations ( $\Phi = 0^\circ$  and  $90^\circ$ ) indicates the surface is highly anisotropic. From the SF spectra, we can obtain a qualitative picture for the orientation of the NH group. The NH vibrational mode is most strongly excited by fields along  $\hat{\zeta}$ , and therefore  $a_{\text{NH},\zeta\zeta\zeta}$  is the strongest element in the nonlinear polarizability of NH,  $\vec{a}_{\text{NH}}$ . The SSS signal at  $\Phi = 0^\circ$  is much stronger than that at  $\Phi = 90^\circ$ , indicating that the NH bond is aligned nearly perpendicular to the rubbing direction ( $\hat{x}$ ). The much stronger SSS than PPS signal suggests that the NH bond lies close to the surface plane. More quantitatively, the

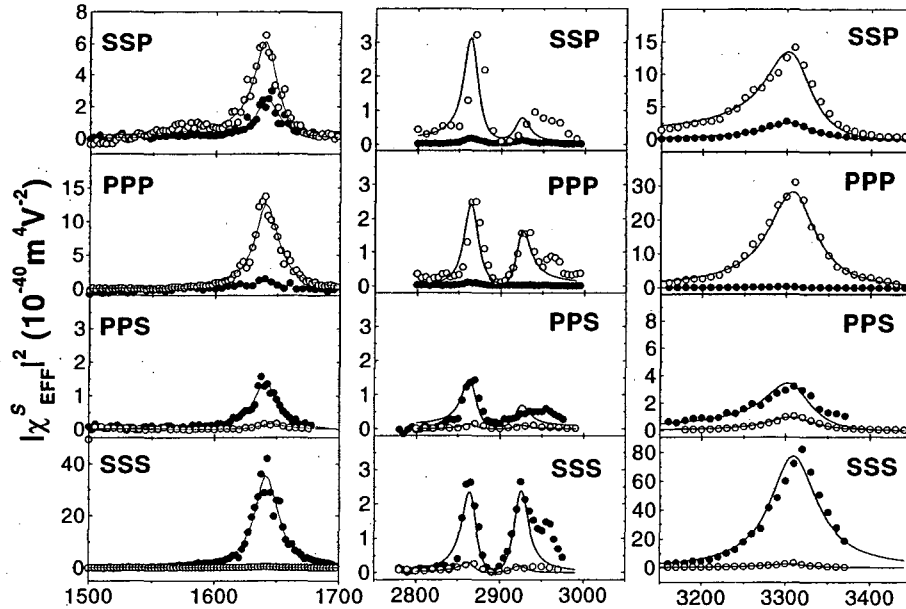


Figure 6.3: SF spectra of rubbed nylon 11 in the vibration ranges of (a) CO, (b) CH<sub>2</sub>, and (c) NH for different polarization combinations (●:  $\Phi = 0^\circ$  and ○:  $\Phi = 90^\circ$ ). Lines are obtained from fits with the 'calculated'  $A_{q,EFF}$ .

SF measurements for rubbed nylon 11 enable us to determine the orientational distribution of the molecular groups,  $f(\Omega)$ . We can write

$$\chi_{EFF}^S = \chi_{NR,EFF}^S + \sum_q \frac{A_{q,EFF}}{\omega_2 - \omega_q + i\Gamma_q}, \quad (6.1)$$

$$A_{q,EFF} \equiv (\vec{L}(\omega_s) \cdot \hat{e}(\omega_s)) \cdot \vec{A}_q \cdot (\vec{L}(\omega_1) \cdot \hat{e}(\omega_1)) (\vec{L}(\omega_2) \cdot \hat{e}(\omega_2)), \quad (6.2)$$

$$\vec{A}_q \equiv N_s \int \vec{a}_q(\Omega) f(\Omega) d\Omega \quad (6.3)$$

where  $N_s$ ,  $\chi_{NR,EFF}^S$ ,  $\vec{a}_q$ ,  $\omega_q$ , and  $\Gamma_q$  are the effective surface density of molecules, the nonresonant background, and the strength, resonant frequency, and damping constant, respectively, of the  $q^{\text{th}}$  vibrational mode,  $\Omega$  denotes the Euler angles ( $\theta$ ,  $\phi$ , and  $\psi$ ) that defines the orientation of CH<sub>2</sub> (and also NH and CO), and consequently, the chain of nylon 11 (Fig. 6.1 (c)). Knowing that the SFG signal is proportional to  $|\chi_{EFF}^S|^2$ , we can fit the

observed spectra using Eq. 6.1 and deduce the ‘measured’  $A_{q,\text{EFF}}$  (see Fig. 6.3). On the other hand, we can calculate  $A_{q,\text{EFF}}$  from known  $\vec{a}_q$  and an assumed distribution function

$$f(\Omega) = Ce^{-\frac{(\theta-\theta_0)^2}{2\sigma_\theta^2} - \frac{(\phi-\phi_0)^2}{2\sigma_\phi^2} - \frac{(\psi-\psi_0)^2}{2\sigma_\psi^2}} \quad (6.4)$$

with  $\theta_0$ ,  $\phi_0$ ,  $\psi_0$ ,  $\sigma_\theta$ ,  $\sigma_\phi$ , and  $\sigma_\psi$  as adjustable parameters (for NH and CO, there is no dependence on  $\psi$ ). The results are presented in Table 6.1. To obtain the ‘calculated’  $A_{q,\text{EFF}}$  for the NH groups, we used the measured values of  $\omega_{\text{NH}} = 3314 \text{ cm}^{-1}$  and  $\Gamma_{\text{NH}}/(2\pi c) = 33.5 \text{ cm}^{-1}$ . The NH bond has two nonvanishing independent  $\vec{a}_{\text{NH}}$  elements,  $a_{\xi\xi\zeta}$  ( $= a_{\eta\eta\zeta}$ ) and  $a_{\zeta\zeta\zeta}$ , and we found  $a_{\xi\xi\zeta}/a_{\zeta\zeta\zeta} \sim 0.14$  from Ref. [75]. Then, with the following values of the adjustable parameters

$$\theta_0 = 75^\circ \pm 6^\circ, \quad \phi_0 = 12^\circ \pm 3^\circ, \quad \sigma_\theta = 60^\circ \pm 10^\circ, \quad \sigma_\phi = 32^\circ \pm 10^\circ, \quad (6.5)$$

the ‘calculated’  $A_{\text{NH},\text{EFF}}$  agree with the ‘measured’ ones to within 20 %, except for  $A_{\text{NH},\text{EFF}}(\text{PPP}, //)$  and  $A_{\text{NH},\text{EFF}}(\text{PPS}, //)$  as seen in Table 6.1. With the same values of the orientational parameters for CO and with  $\omega_{\text{CO}} = 1641 \text{ cm}^{-1}$  and  $\Gamma_{\text{CO}}/(2\pi c) = 11 \text{ cm}^{-1}$ , the dominant  $A_{\text{CO},\text{EFF}}$  elements also show fair agreement between the ‘calculated’ and the ‘measured’ values, confirming that the orientations of NH and CO are the same. In the calculation, we used  $(a_{\xi\xi\zeta}/a_{\zeta\zeta\zeta})_{\text{CO}} = 0.14 \pm 0.02$ .

Knowing that NH and CO align horizontally and nearly perpendicularly (off by  $\sim 12^\circ$ ) to the rubbing direction (see Fig. 6.1 (d)), one can estimate the thickness of the polar-ordered layer and the magnitude of the nonlinear polarizability of CO, which is not otherwise known. If the thickness  $l$  of the polar layer is larger than the coherence length,  $l_{\text{coh}}^{\text{R(T)}}$ , for SFG in reflection (R) or transmission (T),  $|\chi_{\text{EFF}}^S|$  at  $\omega_2 = \omega_q$  ( $q$ : NH or CO) for

Table 6.1: Measured and calculated  $A_{q, \text{EFF}}$  of CO, symmetric  $\text{CH}_2$ , anti-symmetric  $\text{CH}_2$ , and NH vibrational modes for different polarization combinations and sample orientations ( $\Phi = 0^\circ$  (//) and  $\Phi = 90^\circ$  ( $\perp$ )) ( $10^{-9} \text{ m}^2 \text{ V}^{-1} \text{ sec}^{-1}$ ).

	CO		<i>s</i> -CH <sub>2</sub>		<i>a</i> -CH <sub>2</sub>		NH		
	measured	calculated	measured	calculated	measured	calculated	measured	calculated	
SSP	//	33.2 ± 5	19.4	7.7 ± 5	7.5	-6.4 ± 5	-3.2	99.5 ± 15	81.2
	$\perp$	51.6 ± 5	43.8	31.7 ± 5	27.4	-16.4 ± 5	-4.9	223 ± 15	187
PPP	//	-23.2 ± 5	-13.8	-5.5 ± 5	-6.3	-3.7 ± 5	-2.9	-30.9 ± 15	-65.4
	$\perp$	-75 ± 5	-86.7	-27.3 ± 5	-24.7	-20.4 ± 5	-10.3	-336 ± 15	-398
PPS	//	-25.1 ± 5	-33.7	-21.3 ± 5	-24.2	14.9 ± 5	3.9	-114 ± 20	-168
	$\perp$	-8.5 ± 5	13	6.8 ± 5	5.3	-6.2 ± 5	-2.2	62.2 ± 15	61
SSS	//	126 ± 5	120	26.2 ± 5	30.5	26.4 ± 10	14.9	558 ± 20	506
	$\perp$	-12.6 ± 5	-18.9	-8.9 ± 5	-6.3	-7.9 ± 5	-4.7	-101 ± 15	-79.8

SSS and  $\Phi=0^\circ$  is approximately given by

$$|\chi_{\text{EFF}}^S|(\text{SSS}) \sim |N_v l_{\text{coh}}^{\text{R(T)}} L(\omega_s)_y L(\omega_1)_y L(\omega_2)_y \frac{(\langle \vec{a}_q \rangle_f)_{yyy}}{\Gamma_q}|, \quad (6.6)$$

where  $(\langle \vec{a}_q \rangle_f)_{yyy} \sim \int a_{q,\zeta\zeta\zeta}(\hat{\zeta} \cdot \hat{y})(\hat{\zeta} \cdot \hat{y})(\hat{\zeta} \cdot \hat{y})f(\Omega)d\Omega$  with  $a_{q,\zeta\zeta\zeta}$  dominant. For NH, we used the results of Refs. [75] and [76] to find the values of  $a_{\text{NH},\zeta\zeta\zeta}$ . We calculated  $a_{\text{NH}_3,\zeta'\zeta'\zeta'}$  from Ref. [75] and then the bond-additivity model in Ref. [76] provided the relation between  $a_{\text{NH}_3,\zeta'\zeta'\zeta'}$  and  $a_{\text{NH},\zeta\zeta\zeta}$ , where  $\hat{\zeta}'$  is a symmetric axis of  $\text{NH}_3$  and  $\hat{\zeta}$  an unit vector along the bond direction. We obtained  $a_{\text{NH},\zeta\zeta\zeta} \sim 1.1 \times 10^{-26} \text{ m}^4 \text{ V}^{-1} \text{ sec}^{-1}$ . From Eq. 6.6 using the measured value of  $|\chi_{\text{EFF}}^S|_{\text{NH}}(\text{SSS}, //)$  and  $N_v$ (volume density) =  $2.8 \times 10^{-3} \text{ \AA}^{-3}$  (in a perfect crystal) [77], we found  $l_{\text{coh}}^{\text{R}} \sim 100 \text{ nm}$  which is close to the coherence length for SFG in reflection calculated from the refractive indices of nylon. This indicates that indeed  $l > l_{\text{coh}}^{\text{R}}$ . Since CO is always paired with NH, knowing  $|\chi_{\text{EFF}}^S|_{\text{CO}}(\text{SSS}, //)$  we calculated  $a_{\text{CO},\zeta\zeta\zeta} \sim 2.2 \times 10^{-27} \text{ m}^4 \text{ V}^{-1} \text{ sec}^{-1}$ . In SF transmission measurements [27], we found  $|\chi_{\text{EFF}}^S|_{\text{CO}}(\text{SSS}, //)$  to be  $\sim 13$  times larger than in reflection SFVS, yielding  $l_{\text{coh}}^{\text{T}} \sim 1.3 \text{ \mu m}$  which is also close to the calculated coherence length of  $1.1 \text{ \mu m}$ , suggesting that the actual thickness of the polar layer is  $\sim 1 \text{ \mu m}$  or higher.

The SF results for  $\text{CH}_2$  are somewhat surprising. Even with the symmetric arrangement of the ten  $\text{CH}_2$  groups along the chain, the SF signal from  $\text{CH}_2$  remains strong. Presumably this is because the NH and CO terminals of the  $\text{CH}_2$  section break the symmetry so that the contributions of individual  $\text{CH}_2$  to  $\vec{\chi}$  are not cancelled completely by pairing. In calculating  $A_{q,\text{EFF}}$  for the observed  $\text{CH}_2$  modes, we assume the ratios of the  $a_{\lambda\mu\nu}$  to be the same as those deduced earlier for individual  $\text{CH}_2$  [26] for the symmetric (*s*) and anti-symmetric (*a*) stretch modes. We also used  $\omega_{s-\text{CH}_2} = 2870 \text{ cm}^{-1}$  and  $\omega_{a-\text{CH}_2} = 2929 \text{ cm}^{-1}$ ,

$\Gamma_{s(a)}/(2\pi c) = 9 \text{ cm}^{-1}$ ,  $\psi_0 = 0^\circ$ ,  $\sigma_\psi = 60^\circ$ , and the values of the other orientational parameters in Eq. 6.5. We found that all the ‘calculated’  $A_{s,\text{EFF}}$  agree with the ‘measured’ ones within  $\sim 20\%$ . The value  $\sigma_\psi \sim 60^\circ$  indicates that  $\text{CH}_2$  has a broad  $\psi$  orientation. The discrepancy between measured and calculated values in  $A_{a,\text{EFF}}$  is however large. The problem could be due to the complex structure of the spectra including the presence of an unassigned peak around  $2970 \text{ cm}^{-1}$  or error in the assumption regarding  $a_{\lambda\mu\nu}$ . From the preceding results, we conclude that the nylon chains are aligned nearly parallel along the rubbing direction with the dipoles aligned laterally.

## 6.4 Discussion

The dramatic enhancement of the SF signal in rubbed nylon 11 was explained by rubbing-induced polar ordering. For comparison, we also measured the SF signal from isotropic and rubbed nylon 6 films. The SF signal of isotropic nylon 6 was below the noise level and that of rubbed nylon 6 for the  $\text{CH}_2$  stretch modes in the SSP configuration was barely observable ( $|\chi_{\text{EFF}}^S|_{a, //}^2 \sim 8 \times 10^{-43} \text{ m}^4 \text{ V}^{-2}$ ). We found  $|\chi_{\text{EFF}}^S|_{a, //} : |\chi_{\text{EFF}}^S|_{a, \perp} : |\chi_{\text{EFF}}^S|_{s, //} : |\chi_{\text{EFF}}^S|_{s, \perp} \sim 1. : 0.7 : 0.7 : 0.4$ , implying that there is no strong polar ordering and that the nylon chains at the surface are aligned along the rubbing direction with the  $\text{CH}_2$  symmetric axis (as well as NH and CO) lying towards the surface plane. The amides in both nylon 11 and 6 should be aligned laterally to ensure that all the amide units at the surface are hydrogen-bonded.

An interesting question to ask is why the surface polarization in rubbed nylon 11 points to either left or right with respect to the rubbing direction, which supposedly cannot break the left-right symmetry. The strong transmission SF signal suggests that the rubbed

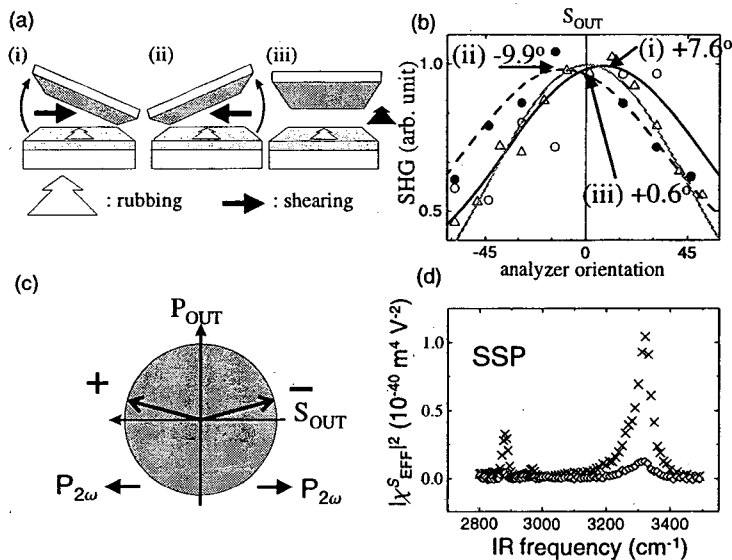


Figure 6.4: (a) Three different shearing directions with respect to the rubbing direction, (b) the dependence of the SHG polarization on the shearing directions ((i):  $\Delta$ , (ii):  $\bullet$ , and (iii):  $\circ$ ) (the maxima were adjusted to be equal), (c) the schematic of the SHG polarizations and the in-plane dipoles in (i) and (ii) ( $P_{2\omega}$ : in-plane SHG dipole), and (d) SF spectra (SSP) of a strongly sheared nylon 11 sample ( $\times$ : along the shearing direction and  $\diamond$ : perpendicular to the shearing direction)

nylon 11 film consists of a single polar domain. In order to check the asymmetry of the dipole alignment and find a possible mechanism for the symmetry breaking, we prepared three different samples with three relative orientations between ‘shearing’ and rubbing as shown in Fig. 6.4 (a). Shearing of the sample surface from the OTS-coated glass was weak enough not to create any noticeable polar ordering or anisotropy. We used second harmonic generation (SHG) to probe polar ordering induced by rubbing. In Fig. 6.4 (b), the position of the analyzer yielding the maximum SHG output determines the polarization of the SHG. The departures of the analyzer orientation for the maximum SHG from  $0^\circ$  ( $S_{OUT}$ ) as shown in Fig. 6.4 (b) ((i) and (ii)) indicates that the polarization of SHG output deviates from  $S_{OUT}$  as shown in Fig. 6.4 (c). The samples with opposite lateral shears

((i) and (ii)) yielded S-polarized components of SHG ( $S_{\text{OUT}}$ )  $180^\circ$  out of phase, while the P-polarized components ( $P_{\text{OUT}}$ ) of the two are the same (Fig. 6.4 (b), (c)). These samples apparently have opposite dc polarization pointing in opposite directions nearly perpendicular to rubbing. In the sample with the parallel shear (iii), the maximum SHG output was obtained when the analyzer orientation is  $\sim 0^\circ$  ( $S_{\text{OUT}}$ ), presumably because the surface was composed of opposite ferroelectric domains, the size of which is suggested to be larger than the wavelength of the light but smaller than the beam size at the sample so that the contributions from individual domains can be added incoherently and yield the maximum SHG at the analyzer angle of  $\sim 0^\circ$ . The determination of the domain size will be conducted in the future. The correlation between the shearing and dipole directions suggests the initial shear is responsible for the symmetry breaking. With a harder shearing of unrubbed samples, dc polarizations appears to align along the shearing direction (Fig. 6.4 (d)). It seems that some amide moieties adsorbed to the template were pulled along the shearing direction upon sample separation from the cover plate and the surface was polarized along that direction.

## 6.5 Conclusions

We have shown that rubbing can create strong polar ordering at the nylon 11 surface. The chains align nearly along the rubbing direction and the dipoles perpendicularly to the rubbing direction forming a lateral ferroelectrically-ordered structure. A possible mechanism for symmetry breaking is identified as due to sample shearing involved in sample preparation.

## Appendix A

# Scanning force microscopy on nylon surfaces

We also investigated the nylon surfaces using scanning force microscopy (SFM). SFM is able to show the morphology and tribological properties of polymers [25, 78]. A recent development of scanning polarization force microscopy (SPFM) and kelvin probe microscopy (KPM) enables us to probe surface polarization by measuring surface potentials [35]. With SPFM/KPM, the vertical polarization of rubbed nylon 11 was examined and found to be less than our detection sensitivity, indicating the polarization should be in the plane, consistent with the SFVS result.

We used a home-built force microscope operated by electronic controllers from RHK Technology, Inc. in two different modes: contact AFM and scanning polarization force microscopy/kelvin probe microscopy (SPFM/KPM). The schematic for SPFM/KPM is shown in Fig. A.1. Contact-mode AFM was used to image the topography of surfaces.

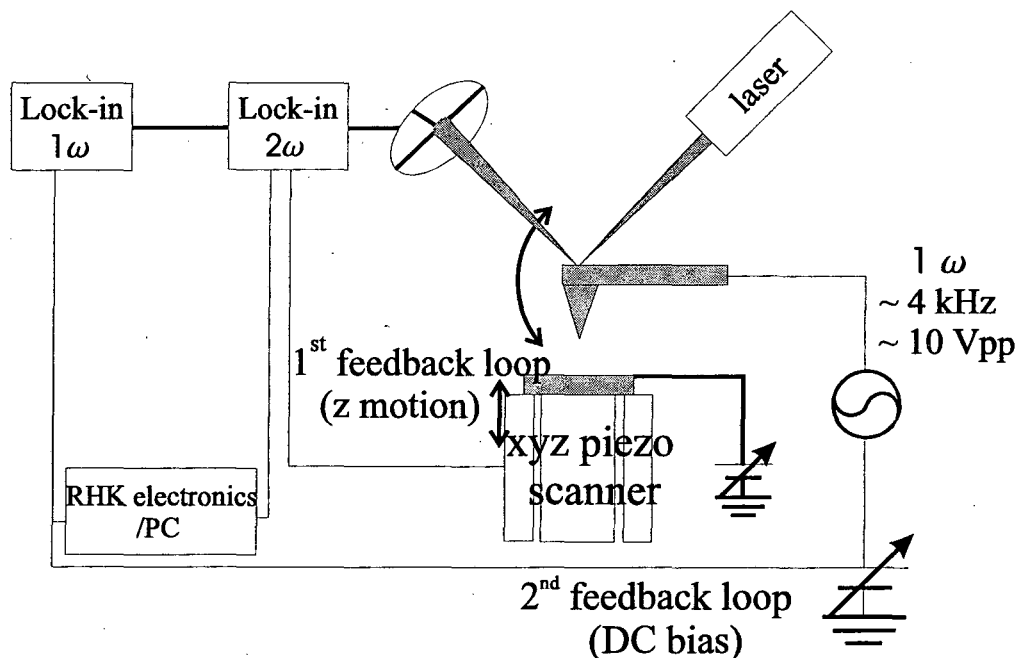


Figure A.1: Schematic diagram of SPFM/KPM setup

The tip from Nanosensor, Inc. is made of Si with a force constant  $0.07 \sim 0.4$  N/m (typically,  $k \sim 0.2$  N/m). A laser beam reflected from the back of the cantilever is directed to a position sensitive detector (PSD) with 4 quadrants and used to monitor the position of the cantilever. The signal differences between top and bottom and between left and right determine the vertical force and the lateral positions, respectively. The typical scan size is up to  $6 \mu\text{m} \times 6 \mu\text{m}$ , and the scan speed is less than or around 1 sec/line. The vertical and lateral resolution is as good as a few  $\text{\AA}$  and a few nm, respectively.

In SPFM/KPM, the cantilever is conductive with metallic coating of PtIr<sub>5</sub>. An AC potential oscillating at  $\omega$  is applied to the tip, and the vibration of the tip is monitored.

The signal has three frequency components: 0 (DC),  $\omega$ , and  $2\omega$ , as shown below.

$$\begin{aligned}
 F &= A ((V_0 + V_1 \cos \omega t) - \varphi)^2 \\
 &= A (V_1^2 \cos^2 \omega t + 2V_1(V_0 - \varphi) \cos \omega t + (V_0 - \varphi)^2) \\
 &\equiv F(2\omega) + F(1\omega) + F(0\omega)
 \end{aligned} \tag{A.1}$$

where  $V = V_0 + V_1 \cos \omega t$  is the potential applied to the tip,  $\varphi$  a surface potential existing on the sample,  $A = -4 \pi \epsilon_0 \frac{\epsilon-1}{\epsilon+1} \times f(\frac{R}{z})$ , and  $f(\frac{R}{z})$  a function of the tip size ( $R$ ) and the distance ( $z$ ) of the tip from the surface. The  $\omega$  and  $2\omega$  signals are separated by two lock-in amplifiers. The  $2\omega$  signal is kept constant by adjusting  $z$  in  $A$  (1<sup>st</sup> feedback). The spatial distribution of the voltage applied to the  $z$  piezo-scanner then yields the ‘topographic image’ convoluted with the local dielectric constant  $\epsilon$ . The  $\omega$  signal is kept at zero by feedback equalizing  $V_0$  to local  $\varphi$  (2<sup>nd</sup> feedback). From the feedback signal  $V_0$ , we can determine  $\varphi$ . Thus, the ‘topography’ and surface potential of the surface can be determined separately. In our experiment, we applied  $V_1 \sim 10$  V and  $\frac{\omega}{2\pi} = 4$  kHz which is far from the resonance of the cantilever. The lateral resolution is about the distance between the tip and the surface, typically  $\sim 20$  nm and the vertical resolution is determined by the noise of the system, typically a few nm. In order to determine the sign of a surface potential, a DC tip bias with a known sign is applied and the sign of the force between the tip and the surface is measured via the direction of the bending of the tip. For calibration, a known DC potential can be applied to a graphite surface (See Fig. A.2). The tip bias is expected to be equal to the applied surface potential.

In a nano-scratching measurement, the sample surface can be scratched by scanning the surface with a rigid metallic tip ( $k \sim 3$  N/m) in contact mode. Afterwards, the

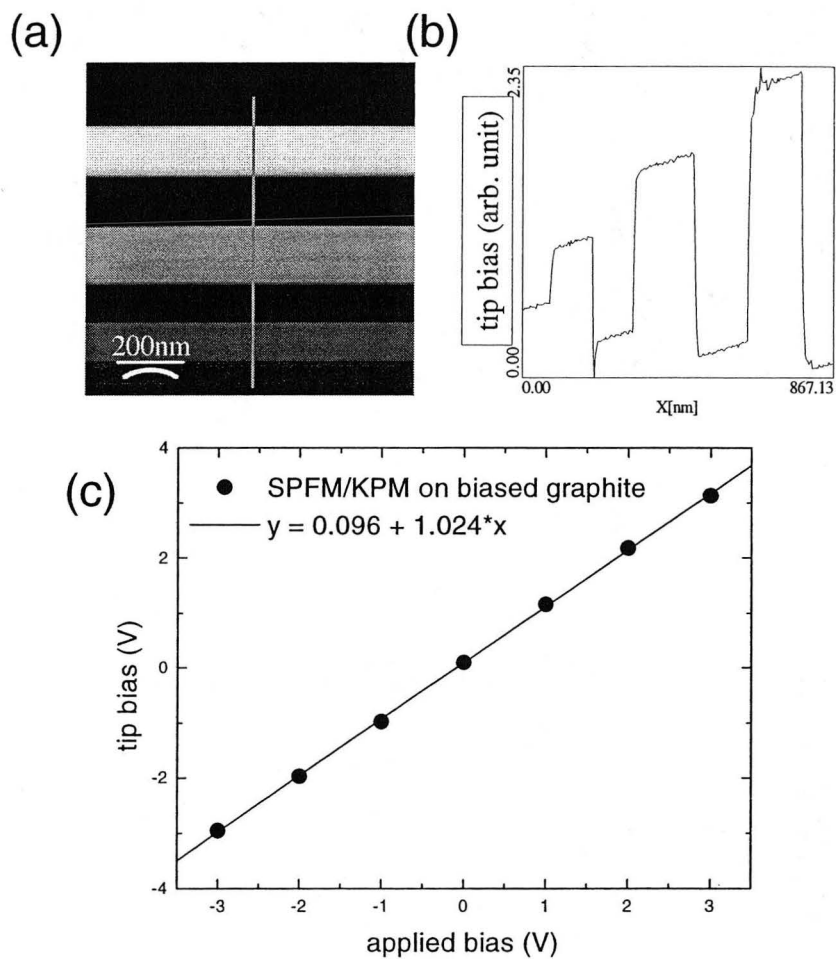


Figure A.2: Calibration of the tip bias with the surface potential at a graphite reference. (a) Tip bias image, (b) a profile along the vertical line segment in (a), and (c) the one-to-one correlation between the tip bias and the applied potential of the graphite.

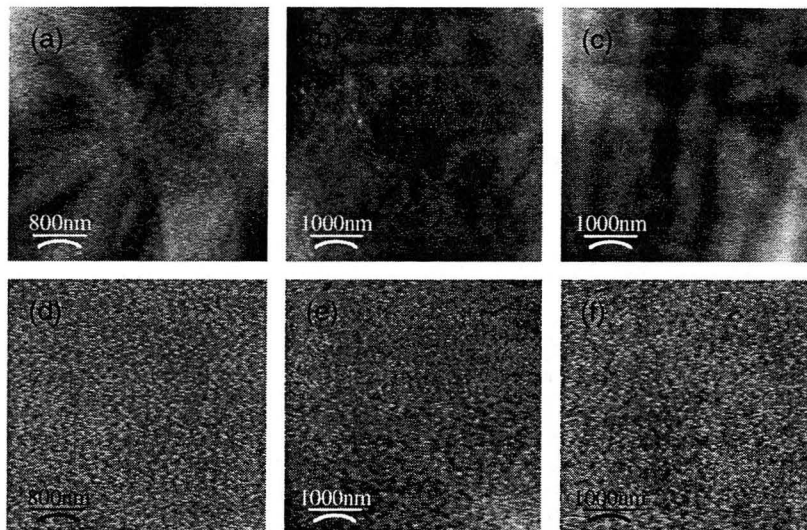


Figure A.3: SPFM/KPM images of rubbed nylon 11 ((a):  $2\omega$ , (d):  $1\omega$ ), isotropic nylon 11 ((b):  $2\omega$ , (e):  $1\omega$ ), and isotropic nylon 6((c):  $2\omega$ , (f):  $1\omega$ ).

surface is scanned with a much weaker force to obtain an image of the modified surface. Contact and SPFM/KPM modes are used to determine the topographical modification and any possible vertical polarization induced by the nano-scratching.

The figures in Fig. A.3 are SPFM/KPM images of rubbed nylon 11, isotropic nylon 11, and isotropic nylon 6. In rubbed nylon 11, we could not get any clear evidence for a vertical polarization to which SPFM/KPM is sensitive. The  $2\omega$  images showing the topography are distinct but the tip bias ( $V_1$ ) images showing the surface potential are similar with no feature. In addition, we created groove patterns on the surface of nylon 11 by scratching it with a hard tip (See Fig. A.4). The topographical grooves with almost equal sub-micron spacing were oriented perpendicularly to the scratching direction. The mechanism for the pattern formation is suggested in Fig. A.4 (b). The larger the applied

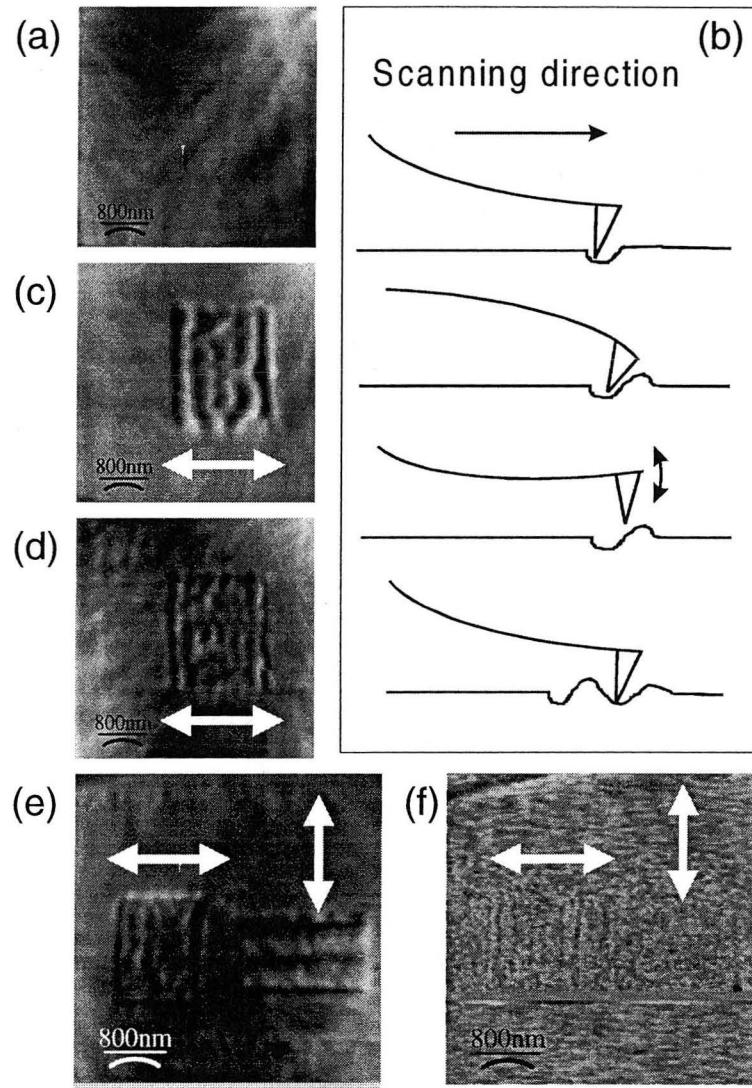


Figure A.4: Formation of groove patterns in nylon 11 by scratching with a hard AFM tip ( $k \sim 3 \text{ N/m}$ ). The image (f) was obtained by SPFM and all others by contact AFM. The arrows in the images indicate the direction of scratching and the orientation of the cantilever was from top to bottom. (a) Nylon 11 before scratching. (b) shows a suggested mechanism for creating grooves by scratching. The applied normal force  $f_N$  during scratching and the approximate spacing  $s$  and depth  $d$  of the grooves are (c)  $f_N = 12.5 \times 10^{-7} \text{ N}$ ,  $s = 350 \text{ nm}$ , and  $d = 30 \text{ nm}$ , (d)  $f_N = 7.5 \times 10^{-7} \text{ N}$ ,  $s = 250 \text{ nm}$ , and  $d = 10 \text{ nm}$ , (e)  $f_N = 5.0 \times 10^{-7} \text{ N}$ ,  $s = 190 \text{ nm}$ , and  $d = 7 \text{ nm}$  for the left image and  $f_N = 5.0 \times 10^{-7} \text{ N}$ ,  $s = 450 \text{ nm}$ , and  $d = 15 \text{ nm}$  for the right image. (f) SPFM image on the same area as in (e)

force is, the wider and the deeper the grooves are. Shown in Fig. A.4 (f) is an image with no clear evidence of surface polarization induced by scratching. In order to verify the lateral polarization observed in chapter 6, we will conduct SFM measurements in a mode sensitive to lateral polarization in the future.

# Bibliography

- [1] L. Stryer, *Biochemistry* 3<sup>rd</sup> ed. (W.H. Freeman, New York, 1988).
- [2] *Applications of polymers*, edited by Raymond B. Seymour and Herman F. Mark (Plenum Press, New York, 1988).
- [3] *Biomedical applications of polymers*, edited by G. E. Zaikov (Nova Science Publishers, Commack, 1999).
- [4] *Conducting polymers, fundamentals and applications : a practical approach*, P. Chandrasekhar (Kluwer Academic, Boston, 1999).
- [5] *Ferroelectric polymers : chemistry, physics, and applications*, edited by Hari Singh Nalwa (M. Dekker Inc., New York, 1995) and references therein.
- [6] *Guidebook to commercial polymers : properties and applications*, N. P. Cheremisinoff (PTR Prentice Hall, Englewood Cliffs, 1993).
- [7] *Liquid crystal polymers : from structures to applications*, A. A. Collyer (Elsevier Applied Science, London, 1992).
- [8] F. S. Bates, G. H. Fredrickson, *Phys. Today*, 32, Feb. 1999.

- [9] C. Galliot, C. Larré, A.-M. Caminade, J.-P. Majoral, *Science*, **277**, 1981 (1997).
- [10] C. K. Chiang, C. R. Jr. Fincher, Y. W. Park, A. J. Heeger, H. Shirakawa, E. J. Louis, S. C. Gau, A. G. MacDiarmid, *Phys. Rev. Lett.* **39**, 1098 (1977).
- [11] J. H. Schön, A. Dodabalapur, Z. Bao, Ch. Kloc, O. Schenker, B. Batlogg, *Nature* **410**, 189 (2001).
- [12] J. H. Burroughes, D. D. Bradley, A. R. Brown, R. N. Marks, K. Mackay, R. H. Friend, P. L. Burns, A. B. Holmes, *Nature* **347**, 539 (1990).
- [13] L. S. Roman, M. Berggren, O. Inganäs, *Appl. Phys. Lett.* **75**, 3557 (1999).
- [14] M. G. Broadhurst, G. T. Davis, J. E. McKinney, R. E. Collins, *J. Appl. Phys.* **49**, 4992 (1978); G. T. Davis, J. E. McKinney, M. G. Broadhurst, S. C. Roth, *J. Appl. Phys.* **49**, 4998 (1978).
- [15] J. W. Lee, Y. Takase, B. A. Newman, J. I. Scheinbeim, *J. Poly. Sci. & Polym. Phys.* **29**, 273 (1991); J. W. Lee, Y. Takase, B. A. Newman, J. I. Scheinbeim, *J. Poly. Sci. & Polym. Phys.* **29**, 279 (1991).
- [16] R. Nakaoka, T. Tsuchiya, K. Sakaguchi, A. Nakamura, *J. Biomed. Mater. Res.* **57**, 279 (2001) and references therein.
- [17] T. Nakano, Y. Satoh, Y. Okamoto, *Macromolecules* **34**, 2405 (2001); F. Wakui, Ph.D. thesis, University of California, Irvine (1991), unpublished and references therein.
- [18] M. H. Litt, C.-H. Hsu, P. Basu, *J. Appl. Phys.* **48**, 2208 (1977).
- [19] B. A. Newman, P. Chen, K. D. Pae, J. I. Scheinbeim, *J. Appl. Phys.* **51**, 5161 (1980).

- [20] V. Gelfandbein, D. Katz, *Ferroelectrics* **33**, 111 (1981).
- [21] J. I. Scheinbeim, *J. Appl. Phys.* **52**, 5939 (1981).
- [22] Y. Takase, J. W. Lee, J. I. Scheinbeim, B. A. Newman, *Macromol.* **24**, 6644 (1991).
- [23] K. Shirota, M. Yaginuma, T. Sakai, K. Ishikawa, H. Takezoe, A. Fukuda, *Appl. Phys. Lett.* **69**, 164 (1996); T. Sakai, J. Yoo, Y. Kinoshita, K. Ishikawa, H. Takezoe, A. Fukuda, T. Nihira, H. Endo, *Appl. Phys. Lett.* **71**, 2274 (1997).
- [24] D. Zhang, Y. R. Shen, G. A. Somorjai, *Chem. Phys. Lett.* **281**, 394 (1997); D. Zhang, D. H. Gracias, R. Ward, M. Gauckler, Y. Tian, Y. R. Shen, G. A. Somorjai, *J. Phys. Chem. B*, **102**, 6225 (1998).
- [25] D. H. Gracias, D. Zhang, L. Lianos, W. Ibach, Y. R. Shen, G. A. Somorjai, *Chem. Phys.* **245**, 277 (1999); D. H. Gracias, D. Zhang, Y. R. Shen, G. A. Somorjai, *Tribol. Lett.* **4**, 231 (1998).
- [26] X. Wei, X. Zhuang, S.-C. Hong, T. Goto, and Y. R. Shen, *Phys. Rev. Lett.* **82**, 4256 (1999); X. Wei, S.-C. Hong, X. Zhuang, T. Goto, and Y. R. Shen, *Phys. Rev. E* **62**, 5160 (2000).
- [27] X. Wei, S.-C. Hong, A. I. Lvovsky, H. Held, and Y. R. Shen, *J. Phys. Chem. B* **104**, 3349 (2000).
- [28] M. Oh-e, S.-C. Hong, Y. R. Shen, *J. Phys. Chem. B* **104**, 7455 (2000).
- [29] M. Oh-e, A. I. Lvovsky, X. Wei, and Y. R. Shen, *J. Chem. Phys.* **113**, 8827 (2000).

- [30] S.-C. Hong, M. Oh-e, X. Zhuang, Y. R. Shen, J. J. Ge, F. W. Harris, S. Z. D. Cheng, *Phys. Rev. E* **63**, 051706 (2001).
- [31] M. Oh-e, D. Kim, Y. R. Shen, *J. Chem. Phys.* **115**, 5582 (2001).
- [32] D. Kim, M. Oh-e, Y. R. Shen, *Macromolecules* **34**, 9125 (2001).
- [33] M. Oh-e, S.-C. Hong, Y. R. Shen, *Appl. Phys. Lett.* **80**, 784 (2002).
- [34] M. G. Samant, J. Stöhr, H. R. Brown, T. P. Russell, J. M. Sands, S. K. Kumar, *Macromolecules* **29**, 8334 (1996); K. Weiss, C. Wöll, E. Böhm, B. Fiebranz, G. Forstmann, B. Peng, V. Scheumann, D. Johannsmann, *Macromolecules* **31**, 1930 (1998); J. Stöhr, M. G. Samant, A. Cossy-Favre, J. Diaz, Y. Momoi, S. Odahara, T. Nagata, *Macromolecules* **31**, 1942 (1998); A. Cossy-Favre, J. Diaz, Y. Liu, H. R. Brown, M. G. Samant, J. Stöhr, A. J. Hanna, S. Anders, T. P. Russell, *Macromolecules* **31**, 4957 (1998).
- [35] L. Xu, M. Salmeron; in *Nano-Surface Chemistry*, edited by M. Rosoff (Marcel Dekker, New York, 2002) and references therein.
- [36] Y. R. Shen, in *Frontiers in Laser Spectroscopy, Proceedings of the International school of Physics "Enrico Fermi"*, Course CXX, edited by T. W. Hansch and M. Inguscio (North-Holland, Amsterdam, 1994), p. 139.
- [37] X. Wei, Ph.D. thesis, University of California, Berkeley (2000), unpublished.
- [38] J. Hunt, Ph.D. thesis, University of California, Berkeley (1988), unpublished.
- [39] P. B. Miranda, Ph.D. thesis, University of California, Berkeley (1998), unpublished.
- [40] D. Kim, Ph.D. thesis, University of California, Berkeley (1997), unpublished.

- [41] Y. R. Shen, *Annu. Rev. Phys. Chem.* **40**, 327 (1989).
- [42] M. B. Feller, Ph.D. thesis, University of California, Berkeley (1991), unpublished.
- [43] W. Chen, M. B. Feller, and Y. R. Shen, *Phys. Lett.* **63**, 2665 (1989); M. B. Feller, W. Chen, and Y. R. Shen, *Phys. Rev. A* **43**, 6778 (1991).
- [44] C. Mauguin, *Bull. Soc. Fr. Miner.* **34**, 71 (1911).
- [45] B. Bahadur, ed., *Liquid Crystals Applications and Uses* (World Scientific, Singapore, 1990).
- [46] D. W. Berreman, *Phys. Rev. Lett.* **28**, 1683 (1972); *Mol. Cryst. Liq. Cryst.* **23**, 215 (1973).
- [47] J. M. Geary, J. W. Goodby, A. R. Kmetz, and J. S. Patel, *J. Appl. Phys.* **62**, 4100 (1987).
- [48] Y. M. Zhu, L. Wang, Z. H. Lu, Y. Wei, X. X. Chen, and J. H. Tang, *Appl. Phys. Lett.* **65**, 49 (1994).
- [49] Y. B. Kim, H. Olin, S. Y. Park, J. W. Choi, L. Komitov, M. Matuszczyk, and S. T. Lagerwall, *Appl. Phys. Lett.* **66**, 2218 (1995).
- [50] A. J. Pidduck, G. P. Bryan-Brown, S. Haslam, R. Bannister, and I. Kitely, *J. Vac. Sci. Tech. A* **14**, 1723 (1996).
- [51] I. Hirose, *Jap. J. Appl. Phys. Part1* **35**, 5873 (1996).

- [52] K. Sakamoto, R. Arafune, N. Ito, S. Ushioda, Y. Suzuki, and S. Morokawa, *Jap. J. Appl. Phys.* **33**, L1323 (1994); K. Sakamoto, R. Arafune, N. Ito, and S. Ushioda, *J. Appl. Phys.* **80**, 431 (1996).
- [53] R. Hasegawa, Y. Mori, H. Sasaki and M. Ishibashi, *Jap. J. Appl. Phys.* **35**, 3492 (1996).
- [54] R. Arafune, K. Sakamoto, and S. Ushioda, *Appl. Phys. Lett.* **71**, 2755 (1997).
- [55] G. D. Hietpas, J. M. Sands, and D. L. Allara, *J. Phys. Chem. B* **102**, 10556 (1998).
- [56] M. F. Tony, T. P. Russell, J. A. Logan, H. Kikuchi, J. M. Sands, and S. K. Kumar, *Nature* **374**, 709 (1995).
- [57] I. Hirosawa, N. Sasaki, and H. Kimura, *Jap. J. Appl. Phys. Part2* **38**, L583 (1999).
- [58] X. Zhuang, L. Marrucci, and Y. R. Shen, *Phys. Rev. Lett.* **73**, 1513 (1994); M. Barmentlo, R. W. J. Hollering, and N. A. J. M. van Aerle, *Phys. Rev. A* **46**, R4490 (1992).
- [59] C. S. Mullin, P. Guyot-Sionnest, and Y. R. Shen, *Phys. Rev. A* **39**, 3745 (1989).
- [60] X. Zhuang, D. Wilk, L. Marrucci, and Y. R. Shen, *Phys. Rev. Lett.* **75**, 2144 (1995).
- [61] S. Kobayashi, and Y. Imura, *Proc. SPIE* **2175**, 122 (1994); D.-S. Seo, K. Araya, N. Yoshida, M. Nishikawa, Y. Yabe, and S. Kobayashi, *Jpn. J. Appl. Phys.* **34**, L503 (1995).
- [62] D. Johannsmann, H. Zhou, P. Sonderkaer, H. Wierenga, B. O. Myrvold, and Y. R. Shen, *Phys. Rev. E* **48**, 1889 (1993).
- [63] K.-W. Lee, A. Lien, J. H. Stathis, and S.-H. Paek, *Jpn. J. Appl. Phys.* **36**, 3591 (1997); S.-H. Paek, C. J. Durning, K.-W. Lee, and A. Lien, *J. Appl. Phys.* **83**, 1270 (1998).

- [64] V. G. Chigrinov, V. V. Belyaev, S. V. Belyaev, and M. F. Grebenkin, *Sov. Phys. JETP* **50**, 994 (1979).
- [65] J. J. Ge, G. Xue, F. Li, K. W. McCreight, S. Wang, F. W. Harris, S. Z. D. Cheng, X. Zhuang, S.-C. Hong, and Y. R. Shen, *Macromol. Rapid Commun.* **19**, 619 (1998); J. J. Ge, C. Y. Li, G. Xue, I. K. Mann, S. Z. D. Cheng, J. Z. Zhang, D. Zhang, S.-Y. Wang, F. W. Harris, S.-C. Hong, X. Zhuang, Y. R. Shen, *J. Am. Chem. Soc.* **123**, 5768 (2001)
- [66] J. Y. Huang and A. Lewis, *Biophys. J.* **55**, 835 (1989).
- [67] G. Baur, V. Wittwer, and D. W. Berreman, *Phys. Lett.* **56A**, 142 (1976); K. Han, T. Miyashita, and T. Uchida, *Jpn. J. Appl. Phys.* **32**, L277 (1993).
- [68] X. Wei, D. Kim, M. Oh-e, and Y. R. Shen, to be published in *Nonlinear Optics*.
- [69] G. Varsányi, *Assignments for Vibrational Spectra of Seven Hundred Benzene Derivatives* Vol. 1 (John Wiley & Sons, New York, 1974).
- [70] K. S. Gautam, A. D. Schwab, A. Dhinojwala, D. Zhang, S. M. Dougal and M. S. Yeganeh, *Phys. Rev. Lett.* **85**, 3854, (2000).
- [71] K. A. Briggman, J. C. Stephenson, W. E. Wallace, and L. J. Richter, *J. Phys. Chem. B* **105**, 2785, (2000).
- [72] P. Guyot-Sionnest, H. Hsiung and Y. R. Shen, *Phys. Rev. Lett.* **57**, 2963 (1986).
- [73] E. R. Tovey, B. A. Baldo, *J. Biochem. Biophys. Methods* **19**, 169 (1989)
- [74] J. Stacey, P. G. Isaac, chapter 4 in *Methods in Molecular Biology* **28**, 25 (1994)

- [75] V. Pouthier, C. Ramseyer, C. Giardet, *J. Chem. Phys.* **108**, 6502 (1998).
- [76] C. Hirose, N. Akamatsu, and K. Domen, *J. Chem. Phys.* **96**, 997 (1992).
- [77] V. Gelfandbein, D. Katz, *Ferroelectrics* **33**, 111 (1981)
- [78] H. A. Mizes, K.-G. Loh, R. J. D. Miller, S. K. Ahuja, E. F. Grabowski, *Appl. Phys. Lett.* **59**, 2901 (1991).

**ERNEST ORLANDO LAWRENCE BERKELEY NATIONAL LABORATORY  
ONE CYCLOTRON ROAD | BERKELEY, CALIFORNIA 94720**